

Infigratinib is a Reversible Inhibitor and Mechanism-based Inactivator of Cytochrome P450 3A4

Lloyd Wei Tat Tang¹, Jian Wei Teng¹, Ravi Kumar Verma², Siew Kwan Koh³, Lei Zhou^{3,4,5}, Mei Lin Go¹, Hao Fan² and Eric Chun Yong Chan¹

¹Department of Pharmacy, Faculty of Science, National University of Singapore, Singapore

²Bioinformatics Institute (BII), Agency for Science, Technology and Research (A*STAR), Singapore

³Singapore Eye Research Institute (SERI), Singapore

⁴Department of Ophthalmology, Yong Loo Lin School of Medicine, National University of Singapore, Singapore

⁵Ophthalmology and Visual Sciences Academia Clinical Program, Duke-National University of Singapore Medical School, Singapore

Running Title:

Inhibition and Inactivation of CYP3A4 by Infigratinib

Address Correspondence to:

Professor Eric Chun Yong Chan, Department of Pharmacy, National University of Singapore, 18 Science Drive 4, Singapore 117543.

Email: phaccye@nus.edu.sg; Telephone: +65-6516 6137; Fax: +65-6779 1554

Number of Tables	5
Number of Figures	12
Number of References	48
Number of words in the Abstract	246
Number of words in the Significance Statement	80
Number of words in the Introduction	750
Number of words in the Discussion	1493

ABBREVIATIONS

BEH	Ethylene bridged hybrid
CYP3A4	Cytochrome P450 3A4
CYP3A5	Cytochrome P450 3A5
DDI	Drug-drug interaction
FDA	United States Food and Drug Administration
FGFR	Fibroblast growth factor receptor
GSH	Glutathione
G6P	Glucose-6-phosphate
G6PDH	Glucose-6-phosphate dehydrogenase
HPLC	High-performance liquid chromatography
INF	Infigratinib
K_i	Reversible inhibition constant
K_i	Inactivator concentration at half-maximum inactivation rate constant
k_{inact}	Maximum inactivation rate constant
K_m	Michaelis constant
k_{obs}	Observed first-order rate constant of inactivation
LC/MS/MS	Liquid chromatography tandem mass spectrometry

MBI	Mechanism-based inactivation
MD	Molecular dynamics
MI complex	Metabolite-intermediate complex
MRM	Multiple reaction monitoring
OBS	Orthosteric binding site
P450	Cytochrome P450
QTOF	Quadrupole time-of-flight
rhCYP3A4	Recombinant human cytochrome P450 3A4
rhCYP3A5	Recombinant human cytochrome P450 3A5
ROS	Reactive oxygen species
$t_{1/2}$	Half-life

ABSTRACT

Infigratinib (INF) is a promising selective inhibitor of fibroblast growth factor receptors 1-3 that has recently been accorded both orphan drug designation and priority review status by the U.S Food and Drug Administration for the treatment of advanced cholangiocarcinoma. Its propensity to undergo bioactivation to electrophilic species was recently expounded upon. However, other than causing aberrant idiosyncratic toxicities, these reactive intermediates may elicit mechanism-based inactivation (MBI) of cytochrome P450 enzymes (P450). In this study, we investigated the interactions between INF and the most abundant hepatic cytochrome P450 3A (CYP3A). Our findings revealed that apart from being a potent noncompetitive reversible inhibitor of CYP3A4, INF inactivated CYP3A4 in a time-, concentration- and NADPH-dependent manner with K_i , k_{inact} and partition ratio of 4.17 μM , 0.068 min^{-1} and 41 respectively when rivaroxaban was employed as the probe substrate. Co-incubation with testosterone (alternative CYP3A substrate) or ketoconazole (direct CYP3A inhibitor) attenuated the rate of inactivation whereas the inclusion of glutathione and catalase did not confer such protection. The lack of enzyme activity recovery following dialysis for 4 hours and oxidation with potassium ferricyanide, coupled with the absence of the characteristic Soret peak signature collectively substantiated that inactivation of CYP3A4 by INF was not mediated by the formation of quasi-irreversible metabolite-intermediate complexes but rather through irreversible covalent adduction to the prosthetic heme and/or apoprotein. Finally, glutathione trapping and high-resolution mass spectrometry experimental results unravelled two plausible bioactivation mechanisms of INF arising from the generation of a *p*-benzoquinonediimine and epoxide reactive intermediate.

Keywords: infigratinib (BGJ398), CYP3A4, mechanism-based inactivation, reversible inhibition, covalent adduction, reactive metabolite

SIGNIFICANCE STATEMENT

The potential of INF to cause MBI of CYP3A4 was unknown. In this study, we report the reversible noncompetitive inhibition and irreversible covalent MBI of CYP3A4 by INF and proposed two potential bioactivation pathways implicating *p*-benzoquinonediimine and epoxide reactive intermediates. Following which, a unique covalent docking methodology was harnessed to elucidate the structural and molecular determinants underscoring its inactivation. Findings from this study lay the groundwork for future investigation of clinically-relevant drug-drug interactions between INF and concomitant substrates of CYP3A4.

INTRODUCTION

Fibroblast growth factor receptor (FGFR) genomic aberrations have been reported in numerous cancers and are intricately linked to tumour cell proliferation, survival and migration (Haugsten *et al.*, 2010; Turner and Grose, 2010). Consequently, pharmacological ablation of FGFR signalling pathways is rapidly gaining prominence as a promising modality in cancer therapeutics (Dienstmann *et al.*, 2014). To date, two FGFR-selective inhibitors (i.e. erdafitinib and pemigatinib) have already garnered global regulatory approval and a fleet of upcoming FGFR inhibitors – in various phases of drug development – have shown encouraging preclinical and clinical responses (Chae *et al.*, 2017; Markham, 2019; Hoy, 2020). Infigratinib (INF) – formerly designated as BGJ398 (**Fig. 1**), is a highly potent and selective ATP-competitive inhibitor of FGFR1-3 that is currently under clinical investigation for several FGFR-driven cancers (Javle *et al.*, 2018; Botrus *et al.*, 2021). Notably, it has been accorded both orphan drug designation and priority review status by the U.S Food and Drug Administration (FDA) for the treatment of advanced cholangiocarcinoma – a rare malignancy plagued with an extremely poor prognosis and limited therapeutic options (Mosconi *et al.*, 2009).

However, a recent study has identified several putative reactive metabolites of INF that are proposed to have arisen from cytochrome P450 enzyme (P450)-mediated metabolic activation of its *N*-ethyl piperazine and dimethoxybenzene ring moieties (Al-Shakliah *et al.*, 2020). In that regard, the P450s are a ubiquitous family of hemoproteins that serve as one of the major drivers of xenobiotic oxidative metabolism in the human body (Guengerich, 2001; Zanger and Schwab, 2013). It is estimated that just six P450 isoforms contribute to the metabolism of >80% of all marketed drugs (Zanger *et al.*, 2008), thereby entrenching their importance in drug metabolism.

Inadvertently, due to its wide substrate specificities and diversity of reactions that P450s can catalyse, they may also be responsible for metabolic activation of drugs (Guengerich, 2001). These group of reactions are collectively termed as bioactivation and they result in the generation of electrophilic, reactive metabolites that – when liberated – can covalently alkylate to nucleophilic centres on biological macromolecules or generate reactive oxygen species (ROS) leading to oxidative stress (Stephens *et al.*, 2014). These deleterious cellular and molecular perturbations can collectively result in idiosyncratic organ-related toxicities. Inasmuch as the liver is the main site for drug metabolism, it is frequently implicated in bioactivation-mediated toxicities.

Apart from the overt toxicological implications of P450-mediated bioactivation, the reactive intermediate generated can be sequestered within the enzyme and cause mechanism-based inactivation (MBI) via covalent adduction to nucleophilic residues within the apoprotein and/or heme porphyrin ring or through coordination with the heme catalytic iron (Ho *et al.*, 2015). As the loss of enzymatic activity is irreversible and persists *in vivo* even after the inactivator has been systemically cleared from the body – and only restored upon biosynthesis of new enzymes, the extent of endobiotic-xenobiotic interactions and/or drug-drug interactions (DDI) tends to be more profound than with a reversible inhibitor (Bjornsson *et al.*, 2003). Furthermore, MBI of P450 could also lead to autoinhibition of hepatic elimination, time-dependent and/or nonlinear pharmacokinetics. Finally, covalent modification of the P450 protein may constitute neoantigens and trigger adaptive immune responses which can culminate in immune-mediated toxicities (Masubuchi and Horie, 2007). Due to its manifold ramifications in pharmacology and toxicology, it becomes clinically important to discern if a drug elicits MBI of P450.

At this outset, a drug can be characterized as an archetypal MBI of P450 if it exhibits the following features: time- and cofactor-dependency of inactivation, saturable kinetics of inactivation, protection against inactivation by a competing substrate, lack of protection by exogenous nucleophiles or scavengers of ROS, irreversibility of inactivation and a 1:1 binding stoichiometry (Silverman, 1995). Although, the potential for INF to undergo bioactivation has been previously demonstrated, it should be noted that these conclusions were drawn from experiments conducted in rat liver microsomes. Consequently, its propensity to undergo bioactivation and elicit MBI of human P450 remains obfuscated. However, there have been multiple reports of INF accumulation at therapeutic doses in phase I studies (Nogova *et al.*, 2017; Kelly *et al.*, 2019). These clinical observations provided the impetus for us to investigate if INF could elicit any MBI against CYP3A (i.e. CYP3A4/5) – which are known to play a major role in its metabolism (Reyes *et al.*, 2020).

In this study, we revealed for the first time that INF is a potent noncompetitive reversible inhibitor and MBI of CYP3A4. Thereafter, we further demonstrated that INF fulfils all the established criteria for an irreversible MBI and trapped the reactive intermediate responsible for the covalent modification of CYP3A4.

MATERIALS AND METHODS

Chemicals and Reagents. INF and erdafitinib were purchased from MedChem Express (Monmouth Junction, NJ). Dexamethasone, ketoconazole, prednisolone, rivaroxaban, verapamil hydrochloride, glutathione (GSH), catalase safranin O and Tergitol-type NP40 were acquired from Sigma-Aldrich (St. Louis, MO). Midazolam was procured from Tocris Bioscience (Bristol, UK). Testosterone and sodium dithionite was purchased from Tokyo Chemical Industries (Tokyo, Japan). Potassium ferricyanide was obtained from VWR International (Leuven, Belgium). Human recombinant P450 3A4 and 3A5 Supersomes (rhCYP3A4 and rhCYP3A5) co-expressing cytochrome b₅ and NADPH P450 reductase and the NADPH regenerating system comprising NADP⁺ and glucose-6-phosphate (G6P) (NADPH A) and glucose-6-phosphate dehydrogenase (G6PDH) (NADPH B) were purchased from Corning Gentest (Woburn, MA). High performance liquid chromatography (HPLC)-grade acetonitrile was procured from Tedia Company Inc. (Fairfield, OH). Ultrapure water (type I) was obtained using a Milli-Q water purification system (Millipore Corporation, Bedford, MA). All other commercially available chemicals were of analytical or HPLC-grade.

Substrate Depletion of INF in CYP3A4 and CYP3A5. All incubations described in this work were performed in 96-well plates. Incubation mixtures consisting of 20 pmol/mL rhCYP3A4 or rhCYP3A5, 1 μ M INF, G6PDH and 100 mM potassium phosphate buffer (pH 7.4) were prepared in triplicates. After pre-incubating at 37°C for 5 min, the reaction was initiated via the addition of NADP⁺/G6P. The final primary incubation mixture (100 μ L) contained <1% v/v organic solvent. Subsequently, at various time intervals (0, 5, 10, 15, 30, 45, 60, 80 100 and 120 min), an 80 μ L aliquot of each incubation mixture was withdrawn and quenched with equal volumes of ice-cold acetonitrile spiked with 100 nM erdafitinib (internal standard). The quenched

samples were then centrifuged at 4000g at 4°C for 30 min, following which aliquots of the supernatant was withdrawn to quantify the amount of INF remaining using LC/MS/MS.

Time-, Concentration-, and NADPH-dependent Inactivation of CYP3A4. Enzyme inactivation kinetic assays were performed as described in our previous works (Tang *et al.*, 2021a; Tang *et al.*, 2021b). Briefly, primary incubation mixtures comprising 20 – 40 pmol/mL rhCYP3A4, INF (0, 1, 2.5, 5, 15, and 25 μ M), G6PDH and 100 mM potassium phosphate buffer (pH 7.4) were prepared in triplicates. After pre-incubating at 37°C for 5 min, the reaction was initiated via the addition of NADP+/G6P. The final primary incubation mixture (100 μ L) contained <1% v/v organic solvent. Subsequently, at various pre-incubation intervals (0, 3, 8, 15, 22 and 30 min), a 5 μ L aliquot of each primary incubation mixture was sampled and transferred to 95 μ L of pre-warmed secondary incubation mixture consisting of a CYP3A-specific probe substrate, an NADPH regenerating system (1 mM) and 100 mM potassium phosphate buffer (pH 7.4). This yielded a 20-fold dilution. Specifically, three structurally-disparate substrates of CYP3A at concentrations more than ~4 \times their respective K_m were included in our assay (i.e. 200 μ M testosterone, 25 μ M midazolam and 50 μ M rivaroxaban) (**Supplementary Fig. 1**). The secondary incubation mixtures were incubated at 37°C for an additional 10 min (for assays involving testosterone or midazolam) or 2 h (for experiments involving rivaroxaban). After which, an 80 μ L aliquot was immediately withdrawn and quenched with equal volumes of ice-cold acetonitrile spiked with either 1 μ M prednisolone (internal standard for quantification of 6 β -hydroxytestosterone and 1'-hydroxymidazolam) or 4 μ M dexamethasone (internal standard for quantification of hydroxylated rivaroxaban). The quenched samples were centrifuged at 4000g at 4°C for 30 min to obtain the supernatant for LC/MS/MS analysis. Negative control

experiments were performed by substituting NADP+/G6P with 100 mM potassium phosphate buffer (pH 7.4). Additionally, parallel experiments involving rhCYP3A5 in place of rhCYP3A4 were also conducted to investigate if INF exhibits any potential time-dependent inhibition against CYP3A5. The concentrations of the three structurally-disparate probe substrates utilized in these experiments were identical to those employed in the CYP3A4 experiments.

Calculation of MBI Kinetic Parameters (K_I and k_{inact}). To derive the inactivation kinetic parameters (K_I and k_{inact}), the mean of triplicate peak area ratios was used to calculate the natural logarithm of percentage residual P450 enzyme activity normalized to vehicle which was then plotted against pre-incubation time for each INF concentration. The resulting data points were fitted to linear regression and the observed first-order inactivation rate constant (k_{obs}) was derived from the slope of the linear decline in CYP3A activity for each INF concentration. Specifically, in CYP3A MBI assays involving midazolam as the probe substrate, points from pre-incubation timepoints 0 to 15 min were utilized in the derivation of the k_{obs} . Whereas in assays comprising testosterone or rivaroxaban as the probe substrate, points throughout 0 to 30 min were used as the decline in enzymatic activity was determined to be linear even after 30 min of pre-incubation. Following which, a plot of k_{obs} against INF concentrations $[I]$ allowed the fitting of inactivation kinetic parameters (K_I and k_{inact}) to non-linear least square regression based on **Equation 1** in GraphPad 8.0.2 (San Diego, CA)

$$k_{obs} = \frac{k_{inact} \times [I]}{K_I + [I]} \quad (1)$$

where k_{inact} represents the maximal inactivation rate constant; K_i is the concentration of the inactivator at half-maximum inactivation rate constant and $[I]$ is the *in vitro* concentration of the inactivator (INF). **Equation 1** assumes that there is negligible change of $[I]$ during the incubation period and that the loss of enzyme activity purely commensurate with inactivation by INF. The ratio of k_{inact} to K_i was determined by dividing the mean values of k_{inact} by K_i . Lastly, the time required for half of the enzyme molecules to be inactivated ($t_{1/2}$) was determined by **Equation 2**.

$$t_{1/2} = \frac{\ln 2}{k_{\text{inact}}} \quad (2)$$

Partition Ratio. Rivaroxaban was utilized as the probe substrate in the secondary incubation mixture in all subsequent CYP3A4 MBI assays described in this work. Primary incubation mixtures consisting of 100 pmol/mL rhCYP3A4, INF (0, 1, 2.5, 5, 15, 25, and 50 μM), G6PDH and 100 mM potassium phosphate buffer (pH 7.4) were prepared in triplicates. After pre-warming the mixture at 37°C for 5 min, the reaction was initiated via the addition of NADP⁺/G6P and incubated for 45 min to allow inactivation to go into completion. The final primary incubation mixture (50 μL) contained <1% v/v organic solvent. Thereafter, aliquots of the primary incubation mixture were withdrawn and transferred to the secondary incubation mixture (similar to that prepared for the inactivation experiments) and incubated at 37°C for another 2 h. Samples were then quenched and assayed for residual enzyme activity as described above. The partition ratio was estimated as detailed in our previous study (Tang *et al.*, 2021a; Tang *et al.*, 2021b). Briefly, the percentage of residual CYP3A4 activity was plotted against the molar ratio of INF to CYP3A4 concentration. The turnover number (partition ratio + 1) was obtained by extrapolating the intercept of the linear regression line plotted at lower ratios with the straight line plotted at higher ratios

to the abscissa. Finally, the partition ratio was back calculated by subtracting the turnover number by a value of 1.

Substrate Protection. To investigate if enzyme inactivation could be amenable to substrate protection, an alternative CYP3A substrate testosterone, at a concentration of 100 and 200 μM (corresponding to 1:4 and 1:8 molar ratio of INF:testosterone) or a potent direct inhibitor of CYP3A ketoconazole, at a concentration of 0.1 and 1 μM (approximately 1 \times and 10 \times its K_i value), was introduced separately in triplicates to the primary incubation mixture containing 40 pmol/mL rhCYP3A4, 25 μM INF, G6PDH and 100 mM potassium phosphate buffer (pH 7.4). The enzymatic reaction was initiated by the addition of NADP⁺/G6P after pre-incubation at 37°C for 5 min. Aliquots were withdrawn at different pre-incubation time points (0, 3, 8 and 15 min), transferred to the secondary incubation mixture and the mixtures were subsequently assayed for residual CYP3A4 enzymatic activity as described above. Primary incubation mixtures that excluded the addition of either testosterone, ketoconazole or both INF and testosterone or ketoconazole served as the negative controls.

Effect of Exogenous Nucleophile and Scavenger of ROS on Inactivation. The exogenous nucleophilic trapping agent GSH (2 mM) was added to the primary incubation mixture containing 40 pmol/mL rhCYP3A4, 25 μM INF, G6PDH and 100 mM potassium phosphate buffer (pH 7.4). After pre-incubating at 37°C for 5 min, the enzymatic reaction was initiated via the addition of NADP⁺/G6P. At specific pre-incubation time points (0, 3, 8 and 15 min), aliquots were transferred to the secondary incubation mixtures and subsequently assayed for residual CYP3A4 enzymatic activity as previously described. Negative controls were prepared without both INF and GSH or only without GSH in the primary incubation mixture. Parallel experiments involving

the incorporation of catalase (800 U/mL) in place of GSH were also performed to investigate the effects of scavenger of ROS on the inactivation of CYP3A4.

Reversibility of Inactivation. The reversibility of CYP3A4 inactivation was interrogated by two distinct approaches; namely equilibrium dialysis and oxidation by potassium ferricyanide, as described in detail in our previous works (Hong *et al.*, 2016; Karkhanis *et al.*, 2016; Tang *et al.*, 2021b). In the dialysis experiments, triplicate primary incubation mixtures comprising 40 pmol/mL rhCYP3A4, 25 μ M INF, G6PDH and 100 mM potassium phosphate buffer (pH 7.4) were pre-warmed at 37°C for 5 min. Enzymatic reaction was initiated by the addition of NADP+/G6P and allowed to proceed for 30 min. After which, a 5 μ L aliquot was transferred to 95 μ L of the secondary incubation mixture yielding a 20-fold dilution. Concurrently, 90 μ L of the remaining primary incubation mixture was transferred to a Slide-A-Lyzer mini dialysis device (0.1 mL, molecular weight cutoff of 10,000; Pierce Chemical Co., Rockford, IL) and placed in a glass beaker filled with 500 mL of ice-cold 100 mM potassium phosphate buffer (pH 7.4). The buffer system was maintained on ice (4°C) with constant gentle stirring and accompanied by one fresh buffer change at the second hour. After 4 h, 5 μ L of the dialyzed mixture was transferred to each pre-warmed secondary incubation well. All secondary mixtures were further incubated at 37°C for 2 h and subsequently assayed for residual CYP3A4 enzymatic activity as previously described.

Conversely, in the experiments involving potassium ferricyanide, a series of three sequential incubations were conducted. Briefly, the primary incubation comprised 40 pmol/mL rhCYP3A4, G6PDH and 100 mM potassium phosphate buffer (pH 7.4) in the presence or absence of 25 μ M INF. Following initiation of the reaction with the addition of NADP+/G6P and incubation at 37°C for either 0 or 30 min, 20 μ L of the primary

incubation mixture was aliquoted into an equal volume of secondary incubation mixture containing 100 mM potassium phosphate buffer (pH 7.4) with or without 2 mM potassium ferricyanide. The secondary mixtures were then allowed to incubate at 37°C for another 10 min. Thereafter, 10 μ L of the mixture was withdrawn and diluted 10-fold into a tertiary incubation mixture containing 50 μ M rivaroxaban (probe substrate), an NADPH regenerating system (1 mM) and 100 mM potassium phosphate buffer (pH 7.4). The reaction mixture was further incubated at 37°C for another 2 h and subsequently assayed for residual CYP3A4 activity as previously described. The percentage of CYP3A4 metabolic activity remaining after 0 or 30 min incubation with INF compared to the corresponding controls in the absence of INF was calculated using **Equation 3** and **4** respectively.

$$\% \text{ control}_{0 \text{ min}} = \frac{v_{(0 \text{ min}, (+) \text{ INF})}}{v_{(0 \text{ min}, (-) \text{ INF})}} \times 100 \quad (3)$$

$$\% \text{ control}_{30 \text{ min}} = \frac{v_{(30 \text{ min}, (+) \text{ INF})}}{v_{(30 \text{ min}, (-) \text{ INF})}} \times 100 \quad (4)$$

where v represents the residual CYP3A4 activity. Thereafter, % restoration of metabolic activity of CYP3A4 was derived by subtracting % control_{30 min} in the presence of potassium ferricyanide with the corresponding values obtained in the absence of potassium ferricyanide.

Spectral Difference Scanning. Incubation mixtures (200 μ L) containing 200 pmol/mL rhCYP3A4, 25 μ M INF, G6PDH and 100 mM potassium phosphate buffer (pH 7.4) were prepared and pre-incubated at 37°C for 5 min. Thereafter, the enzymatic reaction was initiated via the addition of NADP⁺/G6P and immediately scanned from 400 to 500 nm at 5 min intervals over a 1 h duration using a Hidex Sense microplate reader

(Hidex, Turku, Finland) maintained at a constant 37°C. The spectral differences were obtained by comparing the UV absorbances between the sample and reference wells which consisted of vehicle in place of INF. Positive control wells were also prepared using 10 µM verapamil, a known quasi-irreversible of CYP3A4. Finally, the degree of metabolite-intermediate (MI) complex formation was also quantitatively assessed by measuring the absorbance difference between 454 and 490 nm with time.

Reduced Carbon Monoxide (CO)-Difference Spectroscopy. Reduced CO-difference spectroscopy was performed as previously described (Chan *et al.*, 2012) with slight modifications. Briefly, incubation mixtures (50 µL) comprising 200 pmol/mL rhCYP3A4, 25 µM INF, G6PDH and 100 mM potassium phosphate buffer (pH 7.4) were prepared and pre-warmed at 37°C for 5 min. The enzymatic reaction was then initiated via the addition of NADP+/G6P and allowed to proceed for 30 min. Following which, the reaction was terminated via the addition of 450 µL ice-cold quenching buffer consisting of 1 mM EDTA, 20% glycerol, 1% Tergitol-type NP40, 2 mM safranin O, and 100 mM potassium phosphate buffer (pH 7.4). The quenched mixture was evenly split into two 250-µL tubes (sample and reference tubes) and CO gas was gently bubbled into the sample tube and stopped after about 60 bubbles have been introduced into the mixture. Thereafter, approximately 1 mg of sodium dithionite was added to both tubes and 200 µL of the mixture was transferred out from each tube after gentle inversion into a 96-well plate. The reduced CO-difference spectra for the sample and reference wells were recorded by scanning from 400 to 500 nm using a Hidex Sense microplate reader (Hidex, Turku, Finland). Negative controls were prepared by excluding NADPH from the incubation mixture.

GSH Trapping. GSH trapping experiments were performed as previously outlined (Teng *et al.*, 2010; Hong *et al.*, 2016). Incubation mixtures (500 µL) containing 50

pmol/mL rhCYP3A4, 25 μ M INF, G6PDH, 50 mM GSH and 100 mM potassium phosphate buffer (pH 7.4) were prepared and pre-incubated at 37°C for 5 min. The reaction was then initiated via the addition of NADP⁺/G6P and incubated at 37°C for 1 h. Thereafter, 500 μ L of ice-cold acetonitrile was added to quench the reaction. The resulting mixture was centrifuged at 14,000g at 4°C for 15 min. Following which, the supernatant was transferred to a new microcentrifuge tube and dried under a gentle stream of nitrogen gas (TurboVap LV; Caliper Life Science, Hopkinton, MA). The residue was subsequently reconstituted with 60 μ L of ACN-water mixture (3:7), vortexed and centrifuged at 14,000g at 4°C for 15 min. The supernatant was then carefully removed for LC/MS/MS analysis. Samples which omitted the inclusion of INF in the incubation mixture served as the negative controls.

Covalent Docking of INF to CYP3A4 and CYP3A5. Covalent docking of INF to CYP3A4 and CYP3A5 was performed as described in our previous works (Tang *et al.*, 2021b; Tang *et al.*, 2021c). Briefly, three-dimensional coordinates of INF were obtained from the PubChem database (Kim *et al.*, 2018), from which the *p*-benzoquinonediimine intermediate was derived using LigPrep (Schrödinger, New York) and covalently docked to CYP3A4 and CYP3A5 using CovDock (Zhu *et al.*, 2014) in the Schrödinger suite. The protein dataset for CYP3A4 was composed of the previously curated 49 high-resolution crystal structures (<3 Å) (Tang *et al.*, 2021b), whereas the protein dataset for CYP3A5 consisted of the two reported crystal structures and an ensemble of 28 molecular dynamics (MD) simulation frames generated from our previous trajectory clustering analyses (Tang *et al.*, 2021c).

Reversible Inhibition of CYP3A4 by INF. The reversible inhibition of INF against CYP3A4 was also investigated using the same three structurally-distinct CYP3A probe substrates as described in the MBI assays above. Reaction mixtures for IC₅₀

experiments consisted of either 10 – 20 pmol/mL rhCYP3A4, INF (0.01 – 50 μ M), probe substrate (50 μ M testosterone, 3 μ M midazolam or 10 μ M rivaroxaban – representing concentrations at their respective K_m values), G6PDH and 100 mM potassium phosphate buffer (pH 7.4). Whereas reaction mixtures for K_i experiments comprised 20 pmol/mL rCYP3A4, INF (0, 0.03, 0.06, 1 and 3 μ M), rivaroxaban (2.5, 5, 15 and 30 μ M), G6PDH and 100 mM potassium phosphate buffer (pH 7.4). After pre-warming at 37°C for 5 min, the reaction was initiated via the addition of NADP+/G6P, yielding a final primary incubation mixture (100 μ L) with <1% v/v organic solvent. The reaction mixture was incubated at 37°C for 10 min (for assays involving testosterone or midazolam) or 2 h (for experiments involving rivaroxaban). Following which, aliquots of the samples were quenched, centrifuged and subjected to LC/MS/MS analysis for the quantitation of either 6 β -hydroxytestosterone, 1'-hydroxymidazolam or hydroxylated rivaroxaban.

Calculation of Reversible Inhibition Kinetic Parameters (IC₅₀ and K_i) and Determination of Modes of Inhibition. The IC₅₀ was determined using the log(inhibitor) vs. response – variable slope (four parameters) model based on **Equation 5** in GraphPad 8.0.2 (San Diego, CA)

$$Y = \min + \frac{(\max - \min)}{(1 + 10^{(\log IC_{50} - [I]) \times \text{Hill Slope}})} \quad (5)$$

where IC₅₀ represents the half-maximal inhibitory concentration, min is the minimum effect, max is the maximum effect, [I] is the *in vitro* concentration of the reversible inhibitor, Hill slope is the Hill coefficient and Y is the % enzyme activity compared to control.

Apparent K_i values were derived by nonlinear least-square regression analysis of hydroxylated rivaroxaban formation data (expressed in peak area ratio) collected at various rivaroxaban and INF concentration using **Equation 6** for noncompetitive inhibition in GraphPad 8.0.2 (San Diego, CA). The mode of reversible inhibition was determined based on statistical evaluation of the Michaelis-Menten plots by corrected Akaike's information criterion and further verified via visual inspection of the transformed Lineweaver-Burk plots

$$v = \frac{V_{\max}}{\left(1 + \frac{[I]}{K_i}\right) \times \left(1 + \frac{K_m}{[S]}\right)} \quad (6)$$

where v is the rate of enzyme activity, V_{\max} (maximum rate of reaction) and K_m (Michaelis constant) are kinetic constants for substrate metabolism; $[S]$ is the *in vitro* concentration of substrate (rivaroxaban); $[I]$ is the *in vitro* concentration of inhibitor (INF) and K_i is the equilibrium dissociation constant for the enzyme–inhibitor complex.

Measurement of INF and Residual P450 Activity by LC/MS/MS. All samples were analysed using the liquid chromatography tandem mass spectrometry (LC/MS/MS) system consisting of an Agilent 1290 Infinity ultra-high pressure liquid chromatography (Agilent Technologies Inc., Santa Clara, CA) interfaced with an AB SCIEX QTRAP 3500 tandem mass spectrometry (MS/MS) (AB SCIEX, Framingham, MA). Chromatographic separation of INF and erdafitinib (internal standard) in the substrate depletion assay was achieved with an ACQUITY UPLC ethylene bridged hybrid (BEH) C₁₈, 1.7 μ M, 2.2 \times 100 mm column (Waters, Milford, MA) while a similar but shorter 50 mm column was utilized for the chromatographic separation of the rest of the analytes and internal standards described in this work. The aqueous mobile phase (A) was 0.1% formic acid in water, whereas the organic mobile phase (B) was 0.1% formic acid

in acetonitrile. Mobile phases were delivered at a flow rate of 0.5 mL/min. The column and sample temperature were set at 45°C and 4°C respectively. The gradient elution conditions were as follows: linear gradient from 20 to 80% B (0 – 1.20 min), isocratic at 100% B (1.21 – 2.00 min) and isocratic at 20% B (2.01 – 2.50 min). All analytes were detected in positive electrospray ionization (ESI) mode. The source-dependent MS parameters were as follows: ion spray voltage = 5500 V; source temperature = 500°C; curtain gas (CUR) = 25 psi; ion source gas 1 (sheath gas) = 30 psi; ion source gas 2 (drying gas) = 30 psi. The MRM transitions and compound-dependent MS parameters of the analytes are summarized in **Supplementary Table 1**. Chromatographic peak integration was performed using Analyst software version 1.6.2 (Applied Biosystems). For all LC/MS/MS analyses, the peak area of the analyte was expressed as a ratio to the peak area of the internal standard.

Detection of GSH Adducts. GSH adduct of putative reactive electrophilic intermediate of INF was analysed using the LC/MS/MS system consisting of an Agilent 1290 Infinity ultra-high pressure liquid chromatography (Agilent Technologies Inc., Santa Clara, CA) interfaced with an AB SCIEX QTRAP 5500 MS/MS (AB SCIEX, Framingham, MA). Chromatographic separation was achieved on an ACQUITY UPLC BEH C₁₈, 1.7 µM, 2.2 × 100 mm column (Waters, Milford, MA). The aqueous mobile phase (A) was 0.1% formic acid in water, whereas the organic mobile phase (B) was 0.1% formic acid in acetonitrile. Mobile phases were delivered at a flow rate of 0.45 mL/min. The column and sample temperature were set at 45°C and 4°C respectively. The gradient elution conditions were as follows: linear gradient 5 to 60% B (0 – 6.25 min), isocratic at 95% B (6.26 – 7.00 min) and isocratic at 5% B (7.01 – 8.00 min). An information-dependent acquisition experiment was conducted to detect INF-derived GSH conjugates including precursor ion scan (PIS) of *m/z* 272 in negative ESI mode

and neutral loss scan (NL) of 129 Da in positive ESI mode. Enhanced product ion (EPI) scan was subsequently performed for all potential GSH adducts identified. The source-dependent MS parameters utilized were as follows: ion spray voltage = 5000 V; source temperature = 650°C; curtain gas (CUR) = 20 psi; ion source gas 1 (sheath gas) = 45 psi; ion source gas 2 (drying gas) = 60 psi.

Accurate mass measurement of the prospective INF-derived GSH adduct identified in the GSH trapping experiments was performed using an ACQUITY UPLC system (Waters, Milford, MA) coupled to a quadrupole time-of-flight (QTOF) high resolution MS (AB SCIEX TripleTOF 5600 MS; AB SCIEX, Framingham, MA) equipped with a DuoSpray ion source (AB SCIEX, Framingham, MA). Chromatographic separation was achieved on an ACQUITY UPLC BEH C₁₈, 1.7 μM, 2.2 × 100 mm column (Waters, Milford, MA). The mobile phases, flow rate, temperature and gradient elution conditions were identical to those employed in the LC/MS/MS experiments described earlier in this section. External mass calibration was performed at the start and after every five samples with the APCI Positive Calibration Solution (AB SCIEX, Framingham, MA) to ensure high mass accuracy and reproducibility. Other source-dependent MS parameters are as follows ion spray voltage floating = 5500 V; source temperature = 500°C; CUR = 30 psi; ion source gas 1 (sheath gas) = 55 psi; ion source gas 2 (drying gas) = 60 psi. Whereas the collision energy was set to 38 V with a collision energy spread of 5 V. The QTOF-MS data were extracted and analysed using the PeakView software version 2.2 (AB SCIEX, Framingham, MA).

RESULTS

INF Substrate Depletion by CYP3A4 and CYP3A5. To elucidate any potential time-dependent inhibition of CYP3A by INF, we first monitored the depletion of INF over time by CYP3A4 and CYP3A5. Our results demonstrated that both CYP3A isoforms were capable of metabolizing INF, but with vastly different efficiencies. Specifically, the percentages of INF remaining after 2 h were 34.54 ± 1.33 % in CYP3A4 incubations (**Fig. 2A**) and 81.34 ± 1.80 % in CYP3A5 incubations (**Fig. 2B**). Interestingly, two distinct phases were observed in the log-transformed substrate depletion profile of INF for CYP3A4 but not with CYP3A5 (**Fig. 2C and D**). A comparison of the elimination rate constants in the initial portion of incubation revealed that INF was metabolized ~12 times faster by CYP3A4 as compared to CYP3A5 (i.e. $k_{\text{CYP3A4}} = 0.0200 \pm 0.0009 \text{ min}^{-1}$ compared with $k_{\text{CYP3A5}} = 0.0017 \pm 0.0002 \text{ min}^{-1}$). However, after approximately 45 min of incubation there was a drastic reduction in the rate of metabolism by CYP3A4 which point towards of possible time-dependent inhibition.

Time-, Concentration-, and NADPH-dependent Inactivation of CYP3A4. As our earlier substrate depletion experiments hinted that INF could evoke time-dependent inhibition of CYP3A4, we proceeded with a deeper characterization of its inactivation kinetics using the US FDA-recommended CYP3A substrates testosterone and midazolam. In addition to these prototypical substrates, we also adopted rivaroxaban as a clinically-relevant probe substrate of CYP3A. Our findings revealed that INF inactivated CYP3A4 in a time- and concentration-dependent manner for all three probe substrates of CYP3A utilized (**Fig. 3A – C**), with the most profound loss of enzyme activity obtained when 25 μM INF was pre-incubated with CYP3A4 for 30 min. Moreover, the omission of NADPH – which functions as a cofactor in P450-mediated

metabolic reactions – abrogated the loss of CYP3A-mediated testosterone 6 β -hydroxylase and 1'-midazolam hydroxylase activity when pre-incubated with 50 μ M INF for up to 30 min (**Fig. 4A and B**). This apparent dependence on NADPH implied that prior metabolic activation of INF was a key molecular-initiating event leading to the eventual inactivation of CYP3A4. Furthermore, as the k_{obs} determined from the gradients of each of the included concentrations of INF approached a maximum inactivation rate constant (k_{inact}) (**Fig. 3D – F**), it denoted that the loss of CYP3A4 activity elicited by INF followed pseudo-first-order kinetics. At this outset, the inactivation kinetic parameters (K_{I} and k_{inact}) of INF derived from the Kitz-Wilson plot (Kitz and Wilson, 1962) were $3.26 \pm 0.61 \mu\text{M}$ and $0.027 \pm 0.002 \text{ min}^{-1}$ respectively when testosterone was utilized as the probe substrate, $9.03 \pm 2.85 \mu\text{M}$ and 0.088 ± 0.011 respectively when midazolam was harnessed as the probe substrate and $4.17 \pm 0.93 \mu\text{M}$ and $0.068 \pm 0.005 \text{ min}^{-1}$ when rivaroxaban was employed as the probe substrate. This in turn yielded corresponding $k_{\text{inact}}/K_{\text{I}}$ ratios of 8.4, 9.8 and $16.4 \text{ min}^{-1}\text{mM}^{-1}$ and inactivation $t_{1/2}$ of 25.40, 7.85 and 10.12 min respectively. All reported values of K_{I} , k_{inact} , $k_{\text{inact}}/K_{\text{I}}$ ratio and $t_{1/2}$ are summarized in **Table 1**. Conversely, there was a lack of time- or concentration-dependent reduction of CYP3A5 activity by INF in all three probe substrates utilized (**Supplementary Fig. 2A – C**).

Partition Ratio. A titration method previously described (Silverman, 1995) was adopted, which determined the turnover number for the inactivation of CYP3A4 to be ~ 42 (**Fig. 5A**). This in turn corresponded to a partition ratio of 41 (**Table 1**).

Substrate Protection. Inactivation of CYP3A4 by INF was protected in the presence of both an alternative substrate and direct inhibitor of CYP3A. Coincubation with either testosterone (**Fig. 5B**) or ketoconazole (**Fig. 5C**) attenuated the rate of inactivation by INF as illustrated by the diminished rate of enzyme inactivation with time. Furthermore,

the magnitude of substrate protection conferred appeared to be dose-dependent – wherein inactivation was completely abolished when 1 μ M ketoconazole was co-incubated with INF and CYP3A4 in the primary incubation mixture.

Effect of Exogenous Nucleophile and Scavenger of ROS on Inactivation. The incorporation of GSH or catalase had no appreciable effect on the rate of enzyme inactivation elicited by INF. As evident in **Fig. 5D**, CYP3A4 was inactivated to a similar extent in incubation mixtures comprising INF alone.

Reversibility of Inactivation. To establish whether the inactivation of CYP3A4 by INF is quasi-irreversible or irreversible, the specific nature of inactivation was interrogated via equilibrium dialysis and oxidation with potassium ferricyanide. In the former, the magnitude of CYP3A4 activity was not restored after dialysis at 4°C for 4 h (**Fig. 6A**). Rather, the marginal decrease in residual enzyme activity observed post-dialysis could be ascribed to enzymatic degradation that might have occurred during dialysis as confirmed in vehicle control experiments. With regards to the latter, oxidation with potassium ferricyanide after a 30 min pre-incubation with 25 μ M INF restored the metabolic activity of CYP3A4 by a modest 4.8 ± 1.11 % (**Fig. 6B**).

Spectral Difference Scanning. There was a lack of an observable peak in the Soret region (448 – 458 nm) associated with the formation of quasi-irreversible MI complexes when incubation mixtures containing INF and CYP3A4 were scanned from 400 to 500 nm at 5 min intervals for 1 h (**Fig. 7A**) (Polasek and Miners, 2008). Moreover, tracking the increase in absorbance between 454 nm and the isosbestic point at 490 nm further substantiated the lack of MI complex formation with INF (**Fig. 7B**). In contrast, control experiments involving verapamil (a known quasi-irreversible inactivator of CYP3A4) produced an observable Soret peak and a time-dependent

increase in absorbance in the spectral differences between 454 and 490 nm that correlates with the extent of MI complex formation (**Supplementary Fig. 3A and B**).

Reduced CO-Difference Spectroscopy. To determine if the underlying mechanism of inactivation results from destruction of the prosthetic heme, reduced CO-difference spectroscopy was conducted to investigate the ability of CYP3A4 to bind CO. It is well-established that the interaction between CO and ferrous (reduced) form of P450 produces a complex with a spectrally detectable peak at 450 nm (Omura and Sato, 1964). Consequently, any reduction of this peak arising from incubation with INF in a catalytically-competent system hints at possible heme modification. Here, our findings demonstrate that although there was a decrease in the reduced CO binding spectrum after incubation of CYP3A4 with INF in the presence of NADPH it was somewhat marginal (**Fig. 7C**). Taken together, it implied that while a small fraction of the reactive intermediate may irrevocably modify the prosthetic heme (i.e. via covalent alkylation and/or bleaching), it likely did not represent the major mode of inactivation. Rather, the predominant mechanism of inactivation by INF may be due to covalent adduction of the CYP3A4 apoprotein.

GSH Trapping. A GSH trapping assay was subsequently performed by fortifying the reaction mixtures with the nucleophilic trapping agent GSH to search for electrophilic reactive intermediates of INF that may be potentially implicated in the irreversible covalent adduction of the CYP3A4 apoprotein. Two survey scans – namely PIS at m/z 272 in negative mode and NL of 129 Da in positive mode (Baillie and Davis, 1993; Dieckhaus *et al.*, 2005) – were employed. These two well-established survey scans, which monitor the loss of the deprotonated γ -glutamyl-dehydroalanyl-glycine and pyroglutamic acid moiety from GSH respectively, are frequently utilized by pharmaceutical scientists during drug discovery to identify drug candidates that pose

potential metabolic liabilities. One peak suggestive of an INF-derived GSH adduct (retention time: 3.77 min) with an MH⁺ ion at *m/z* of 865 and a characteristic dual chlorine isotopic pattern was detected in both the PIS at *m/z* 272 in ESI negative mode (**Supplementary Fig. 4**) and NL of 129 Da in positive ESI mode (**Supplementary Fig. 5**) but was absent in negative control samples lacking INF. The resultant EPI scan generated from this prospective INF-derived GSH adduct yielded a spectrum that was characteristic of collision-induced dissociation fragmentation of a GSH adduct due to the neutral mass loss of 129 Da corresponding to the loss of a pyroglutamate moiety in GSH (**Supplementary Fig. 4 and 5**). To further confirm the identity of the potential GSH adduct, accurate mass measurements were performed. As expected, we were able to recapitulate the nominal mass patterns generated using the QTRAP-MS when the GSH adduct was subjected to accurate mass measurements using the QTOF-MS. The proposed elemental composition, theoretical and experimental exact *m/z* and mass accuracy (in both Δ Da and Δ ppm) of the GSH adduct are summarized in **Table 2**. Additionally, the accurate mass MS/MS spectrum and proposed fragmentation pattern of the INF-derived GSH adduct are shown in **Fig. 8**.

Covalent Docking of INF to CYP3A4 and CYP3A5. Covalent docking was performed to glean mechanistic insights on the plausible structural determinants underscoring the diverging MBI susceptibilities of CYP3A4 and CYP3A5 by INF. Our bioinformatics analyses previously identified Cys239 in CYP3A4 as an accessible residue for covalent adduction (Tang *et al.*, 2021b). Interestingly, this cysteine was determined to be substituted by a serine in CYP3A5 (i.e. Ser239) (Tang *et al.*, 2021c). Consequently, we directed our focus on these two residues which were located in the vicinity of the F-F' loop – a region of CYP3A4 and CYP3A5, positioned directly above the orthosteric binding site (OBS), that is generally thought to function as a gate to regulate substrate

access to the catalytic heme (Sevrioukova and Poulos, 2013; Benkaidali *et al.*, 2019). Our results revealed that the top covalent docking scores obtained for INF against residue 239 of CYP3A4 (-4.7) and CYP3A5 (-5.4) were comparable (**Table 3**). Moreover, INF binding poses were also found to be similar in both CYP3A isoforms (**Fig. 9A – C**), whereby the 2,6-dichloro-3,5-dimethoxy-phenyl moiety of INF was spatially oriented towards the F-F' loop with a minimum distance $<5 \text{ \AA}$ (**Table 3**). Taken together, our findings suggested that INF has similar propensities to form adducts with Cys239 and Ser239 in CYP3A4 and CYP3A5 respectively.

Reversible Inhibition of CYP3A4 by INF. Finally, our MBI assays also revealed that there was a reduction in residual enzyme activity in the absence of pre-incubation (i.e. at zero pre-incubation time) (**Fig. 3A – C**), thereby hinting that INF could also elicit reversible inhibition of CYP3A4. Consequently, we proceeded to establish its reversible inhibition kinetics to characterize the interactions more comprehensively between INF and CYP3A4. Our findings demonstrated that INF decreased CYP3A4-mediated testosterone 6β -hydroxylation, midazolam 1'-hydroxylation and rivaroxaban hydroxylation in a concentration-dependent manner and yielded a sigmoidal-shaped dose-response curve with IC_{50} values of 2.04 ± 0.29 , 2.91 ± 0.54 and $0.80 \pm 0.08 \mu\text{M}$ respectively (**Fig. 10A – C**) (**Table 4**). Since INF yielded the most potent inhibition of rivaroxaban hydroxylation, we went on to determine the apparent K_i and mode of reversible inhibition using rivaroxaban as the probe substrate. Based on the nonlinear regression analysis and Lineweaver-Burk plots (**Fig. 11A and B**), INF inhibited CYP3A4-mediated rivaroxaban hydroxylation noncompetitively with an apparent K_i of $0.97 \pm 0.06 \mu\text{M}$ (**Table 4**).

DISCUSSION

INF is a promising selective inhibitor of FGFR1-3 that is currently under clinical investigation for advanced cholangiocarcinoma and several other FGFR-linked cancers. While its propensity to undergo bioactivation to electrophilic species was recently expounded upon, it remains obfuscated if INF could also elicit MBI of P450 – a well-established consequence arising from the generation of reactive intermediates that bears profound pharmacokinetic and toxicological significance. Our findings revealed for the first time that INF is a potent noncompetitive reversible inhibitor and irreversible MBI of CYP3A4.

X-ray crystal structures of CYP3A has helped shed insights on the structural basis underpinning its ligand promiscuity (Williams *et al.*, 2004). It is now recognised that the active site of this P450 subfamily possesses considerable bulk and plasticity which allows the simultaneous binding of multiple substrates in different modes (Kenworthy *et al.*, 1999; Ekroos and Sjögren, 2006). As such the biochemical interactions observed with one probe substrate may not accurately reflect those obtained with another (Galetin *et al.*, 2005; Pearson *et al.*, 2007). Consequently, FDA guidelines recommends the use of at least two structurally-disparate CYP3A substrates to evaluate if there are any substrate- or site-dependent effects on enzyme interactions. Here, in addition to both FDA-recommended substrates, we also included rivaroxaban as a probe substrate in our assays. As rivaroxaban is increasingly being co-administered in cancer for prophylaxis and treatment of cancer-associated venous thromboembolism, its adoption as a probe substrate bears clinical significance (Short and Connors, 2014). Our findings revealed that while INF inactivated CYP3A4 in all three probe substrates employed in our assay, there were considerable differences in their corresponding inactivation kinetic parameters (**Table 1**). Specifically, the k_{inact}/K_i

ratio obtained with rivaroxaban was found to be ~2.0- and 1.7-fold higher than that obtained with testosterone and midazolam respectively. These trends in probe-substrate dependency were also recapitulated in our reversible inhibition assays, wherein INF was found to yield the lowest IC_{50} value when rivaroxaban was adopted as the probe substrate (**Table 4**). Taken together, our results indicated that the inhibition and inactivation of CYP3A4-mediated rivaroxaban hydroxylation by INF is expected to be more potent as compared to its FDA-recommended prototypical substrates and reiterates the importance of using a clinically-relevant probe substrate to derive accurate inhibition and/or inactivation kinetic constants for pharmacokinetic DDI studies.

The average unbound steady-state concentration of INF following a clinical dosing schedule of 125 mg daily for 3 weeks on/1 week off was previously reported to be 6.93 nM (Nogova *et al.*, 2017). When juxtaposed with the K_i values obtained in this work – which are in the micromolar range, it is difficult to evaluate and predict the clinical consequence of the MBI of CYP3A4 by INF. However, a comparison of its k_{inact}/K_i ratio (**Table 5**) revealed that although the inactivation potency of INF is eclipsed by other potent MBI (i.e. mibefradil), it was comparable to other clinically-important MBI such as clarithromycin and diltiazem which are known to perpetrate DDIs via inactivation of CYP3A4. Taken together, it implies that a more refined estimation of INF hepatic concentration (i.e. its maximum unbound concentration within human hepatocytes) may be necessary to accurately discern its actual DDI potential. The elucidation of MBI of CYP3A4 in our study further provides a plausible mechanistic basis underpinning previous reports of INF accumulation in phase I clinical trials after chronic dosing (Nogova *et al.*, 2017; Kelly *et al.*, 2019). It is tempting to posit that these instances of time-dependent pharmacokinetics could arise from autoinhibition of its

CYP3A4-mediated clearance pathways although additional studies are needed to substantiate this postulation.

The efficiency of an MBI can be quantitatively assessed by its partition ratio, which is termed as the number of parent drug molecules required to completely inactivate the enzyme. Notably, compounds which possess ratios of <50 are classified as highly efficient inactivators (Lim *et al.*, 2005). Consequently, the partition ratio of 41 suggests that INF is a relatively efficient MBI of CYP3A4. Moreover, we also demonstrated that co-incubation with either testosterone or ketoconazole attenuated the rate of inactivation, implying that enzymatic inactivation by INF occurred within the active site and could be protected in the presence of an alternative substrate or direct inhibitor. Conversely, the lack of protection conferred by GSH or catalase confirmed that the putative reactive metabolite of INF inactivates the enzyme before it is liberated from the active site and ROS is not involved in enzyme inactivation.

While our experimental findings corroborated the MBI of CYP3A4 by INF, some seeding questions pertaining to the specific nature of inactivation remains unanswered. MI complexes, which arise from the formation of dative bonds between the reactive intermediate and the heme ferrous iron, are quasi-irreversible and can be dissociated *in vitro* by dialysis or with potassium ferricyanide. Conversely, enzyme inactivation that proceeds via covalent adduction to either the P450 heme moiety and/or apoprotein is irreversible and cannot be mitigated by both aforementioned experimental approaches. Here, our findings demonstrated that the loss of CYP3A4 activity is irrevocable and could not be recovered after dialysis. Whereas the addition of potassium ferricyanide only restored activity by a modest 4.8% which when interpreted under the context of a published criterion (Watanabe *et al.*, 2007); further dismisses the possibility of MI complex formation. Finally, the absence of a

characteristic Soret peak and the preservation of the reduced CO binding spectrum further augmented our postulations that INF inactivates CYP3A4 via irreversible covalent adduction to the apoprotein.

As mentioned previously, the successful recapitulation of the nominal mass EPI spectral peaks in our high-resolution QTOF-MS (**Supplementary Fig. 4 and 5**) along with mass accuracies well below the mass tolerance threshold of 5 ppm (**Table 2**) gave us confidence in the predicted elemental compositions of the parent and product ions to elucidate the structure of the INF reactive intermediate. Unexpectedly, we did not manage to detect the reactive *p*-benzoquinone metabolite arising from sequential dechlorination, hydroxylation and O-demethylation of the 2,6-dichloro-3,5-dimethoxyphenyl moiety of INF that was reported by Al-Shakliah *et al.* Rather, the presence of the characteristic dual chlorine isotopic pattern in nominal mass measurements of the INF-derived GSH adduct further ascertained that bioactivation of INF by rhCYP3A4 did not involve dechlorination of this moiety (**Supplementary Fig. 4 and 5**). It should be noted that the aforementioned reported bioactivation pathway for INF was established using rat liver microsomes. Consequently, due to possible inter-species differences in P450, INF may not be liable to the same metabolic activation pathways in humans. Rather, our high-resolution MS analyses suggested that the glutathionyl moiety was alkylated directly to the INF core structure. Consequently, we proposed two alternative bioactivation pathways of INF arising from the generation of a *p*-benzoquinonediimine intermediate or an epoxide intermediate (**Fig. 12**). While it is plausible that both reactive species can facilitate subsequent nucleophilic attack by GSH to form the INF-derived GSH adduct, the electron transfer pathway on the phenylenediamine moiety leading to the formation of the *p*-benzoquinonediimine intermediate may be more facile because it is flanked by an electron deficient

pyrimidine ring and a protonated (i.e. electron-withdrawing) piperazine ring which may diminish its susceptibility to P450-mediated epoxidation.

Finally, another major finding in this work is the lack of inactivation of CYP3A5 by INF. Although CYP3A5 shares ~85% sequence homology with CYP3A4, it is now generally accepted that both CYP3A isoforms have varying susceptibilities to MBI. To delineate the structural basis for this dichotomous isoform-specific inactivation profile by INF, we covalently docked the *p*-benzoquinonediimine intermediate of INF to Cys239 in CYP3A4 and Ser239 in CYP3A5. Our findings revealed that INF possesses similar propensities to form adducts with these residues that lie adjacent to the F-F' loop. We also discovered that, unlike in CYP3A4, INF-Ser239 adducts could stabilize two distinct F-F' loop conformations in CYP3A5. Although the F-F' loop is located in proximity to the C-terminal loop in CYP3A4 and CYP3A5 ('closed' conformation) (**Fig. 9A and B**), it could also be oriented further away from the C-terminal loop in CYP3A5 resulting in a wider entrance to the OBS ('open' conformation) (**Fig. 9C**). Taken together, it is plausible that the greater flexibility of the F-F' loop in CYP3A5 could have preserved substrate accessibility to the OBS despite similar susceptibilities to covalent alkylation by INF. These findings are concordant with our previous study involving the uricosuric agent benzbromarone which also elicited MBI of CYP3A in the same isoform-specific manner (Tang *et al.*, 2021c) and are further corroborated by Pearson *et al.*'s study which underscored the key role of Cys/Ser239 in the differential inactivation of CYP3A by raloxifene.

In conclusion, our results demonstrated that INF is a potent uncompetitive inhibitor and MBI of CYP3A4. Furthermore, we also determined the nature of inactivation to be via covalent modification and elucidated the structure of the putative reactive intermediate involved in its irreversible inactivation. Given the relevance of CYP3A

enzymes in drug metabolism coupled with the polymorphic expression of CYP3A5 and the emerging role of INF as a therapeutic agent for FGFR-linked cancers, further studies are warranted to better understand the pharmacogenomic and clinical implications of our findings.

AUTHORSHIP CONTRIBUTIONS

<i>Participated in research design:</i>	Tang, Verma, Fan, Chan
<i>Conducted experiments:</i>	Tang, Teng, Verma, Koh
<i>Contributed new reagents or analytical tools:</i>	Zhou, Go
<i>Performed data analysis:</i>	Tang, Teng, Verma, Fan, Chan
<i>Wrote or contributed to the writing of the manuscript:</i>	Tang, Teng, Verma, Fan, Chan

BIBLIOGRAPHY

- Al-Shakliah NS, Attwa MW, Kadi AA, and AlRabiah H (2020) Identification and characterization of in silico, in vivo, in vitro, and reactive metabolites of infigratinib using LC-ITMS: bioactivation pathway elucidation and in silico toxicity studies of its metabolites. *RSC Adv* **10**:16231–16244.
- Baillie TA, and Davis MR (1993) Mass spectrometry in the analysis of glutathione conjugates. *Biol Mass Spectrom* **22**:319–325.
- Benkaidali L, André F, Moroy G, Tangour B, Maurel F, and Petitjean M (2019) Four Major Channels Detected in the Cytochrome P450 3A4: A Step toward Understanding Its Multispecificity. *Int J Mol Sci* **20**:987.
- Bjornsson TD, Callaghan JT, Einolf HJ, Fischer V, Gan L, Grimm S, Kao J, King SP, Miwa G, Ni L, Kumar G, McLeod J, Obach RS, Roberts S, Roe A, Shah A, Snikeris F, Sullivan JT, Tweedie D, Vega JM, Walsh J, and Wrighton SA (2003) The conduct of in vitro and in vivo drug-drug interaction studies: A Pharmaceutical Research and Manufacturers of America (PhRMA) perspective. *Drug Metab Dispos* **31**:815–832.
- Botrus G, Raman P, Oliver T, and Bekaii-Saab T (2021) Infigratinib (BGJ398): an investigational agent for the treatment of FGFR-altered intrahepatic cholangiocarcinoma. *Expert Opin Investig Drugs* **00**:1–8.
- Chae YK, Ranganath K, Hammerman PS, Vaklavas C, Mohindra N, Kalyan A, Matsangou M, Costa R, Carneiro B, Villaflor VM, Cristofanilli M, and Giles FJ (2017) Inhibition of the fibroblast growth factor receptor (FGFR) pathway: The current landscape and barriers to clinical application. *Oncotarget* **8**:16052–16074.
- Chan ECY, New LS, Chua TB, Yap CW, Ho HK, and Nelson SD (2012) Interaction of lapatinib with cytochrome P450 3A5. *Drug Metab Dispos* **40**:1414–1422.
- Dieckhaus CM, Fernández-Metzler CL, King R, Krolikowski PH, and Baillie TA (2005) Negative ion tandem mass spectrometry for the detection of glutathione conjugates. *Chem Res Toxicol* **18**:630–638.
- Dienstmann R, Rodon J, Prat A, Perez-Garcia J, Adamo B, Felip E, Cortes J, Iafrate AJ, Nuciforo P, and Tabernero J (2014) Genomic aberrations in the FGFR pathway: Opportunities for targeted therapies in solid tumors. *Ann Oncol* **25**:552–563.
- Ekroos M, and Sjögren T (2006) Structural basis for ligand promiscuity in cytochrome P450 3A4. *Proc Natl Acad Sci U S A* **103**:13682–13687.
- Galetin A, Ito K, Hallifax D, and Houston JB (2005) CYP3A4 substrate selection and substitution in the prediction of potential drug-drug interactions. *J Pharmacol Exp Ther* **314**:180–190.
- Guengerich FP (2001) Common and uncommon cytochrome P450 reactions related to metabolism and chemical toxicity. *Chem Res Toxicol* **14**:611–650.
- Haugsten EM, Wiedlocha A, Olsnes S, and Wesche J (2010) Roles of fibroblast growth

- factor receptors in carcinogenesis, *Mol Cancer Res* **8**:1439–1452.
- Ho HK, Chan JCY, Hardy KD, and Chan ECY (2015) Mechanism-based inactivation of CYP450 enzymes: A case study of lapatinib. *Drug Metab Rev* **47**:21–28.
- Hong Y, Chia YMF, Yeo RH, Venkatesan G, Koh SK, Chai CLL, Zhou L, Kojodjojo P, and Chan ECY (2016) Inactivation of human cytochrome P450 3A4 and 3A5 by dronedarone and n-desbutyl dronedarone. *Mol Pharmacol* **89**:1–13.
- Hoy SM (2020) Pemigatinib: First Approval. *Drugs* **80**:923–929.
- Javle M, Lowery M, Shroff RT, Weiss KH, Springfield C, Borad MJ, Ramanathan RK, Goyal L, Sadeghi S, Macarulla T, El-Khoueiry A, Kelley RK, Borbath I, Choo SP, Oh DY, Philip PA, Chen LT, Reungwetwattana T, Van Cutsem E, Yeh KH, Ciombor K, Finn RS, Patel A, Sen S, Porter D, Isaacs R, Zhu AX, Abou-Alfa GK, and Bekaii-Saab T (2018) Phase II study of BGJ398 in patients with FGFR-Altered advanced cholangiocarcinoma. *J Clin Oncol* **36**:276–282.
- Karkhanis A, Lam HY, Venkatesan G, Koh SK, Chai CLL, Zhou L, Hong Y, Kojodjojo P, and Chan ECY (2016) Multiple modes of inhibition of human cytochrome P450 2J2 by dronedarone, amiodarone and their active metabolites. *Biochem Pharmacol* **107**:67–80.
- Kelly CM, Shoushtari AN, Qin LX, D'Angelo SP, Dickson MA, Gounder MM, Keohan ML, Mcfadyen C, Sjoberg A, Singer S, DeMatteo RP, Hwang S, Heinemann MH, Francis JH, Antonescu CR, Chi P, and Tap WD (2019) A phase Ib study of BGJ398, a pan-FGFR kinase inhibitor in combination with imatinib in patients with advanced gastrointestinal stromal tumor. *Invest New Drugs* **37**:282–290.
- Kenworthy KE, Bloomer JC, Clarke SE, and Houston JB (1999) CYP3A4 drug interactions: Correlation of 10 in vitro probe substrates. *Br J Clin Pharmacol* **48**:716–727.
- Kim S, Chen J, Cheng T, Gindulyte A, and He J (2018) PubChem 2019 update: improved access to chemical data. *Nucleic Acids Res* **47**:1102–1109.
- Kitz R, and Wilson IB (1962) Esters of methanesulfonic acid as irreversible inhibitors of acetylcholinesterase. *J Biol Chem* **237**:3245–3249.
- Lim HK, Duczak N, Brougham L, Elliot M, Patel K, and Chan K (2005) Automated screening with confirmation of mechanism-based inactivation of CYP3A4, CYP2C9, CYP2C19, CYP2D6, and CYP1A2 in pooled human liver microsomes. *Drug Metab Dispos* **33**:1211–1219.
- Ma B, Prueksaritanont T, and Lin JH (2000) Drug interactions with calcium channel blockers: Possible involvement of metabolite-intermediate complexation with CYP3A. *Drug Metab Dispos* **28**:125–130.
- Markham A (2019) Erdafitinib: First Global Approval. *Drugs* **79**:1017–1021.
- Masubuchi Y, and Horie T (2007) Toxicological significance of mechanism-based inactivation of cytochrome P450 enzymes by drugs. *Crit. Rev. Toxicol* **37**:389–412

- Mosconi S, Beretta GD, Labianca R, Zampino MG, Gatta G, and Heinemann V (2009) Cholangiocarcinoma. *Crit Rev Oncol Hematol* **69**:259–270.
- Nogova L, Sequist L V., Garcia JMP, Andre F, Delord JP, Hidalgo M, Schellens JHM, Cassier PA, Camidge DR, Schuler M, Vaishampayan U, Burris H, Tian GG, Campone M, Wainberg ZA, Lim WT, LoRusso P, Shapiro GI, Parker K, Chen X, Choudhury S, Ringeisen F, Graus-Porta D, Porter D, Isaacs R, Buettner R, and Wolf J (2017) Evaluation of BGJ398, a Fibroblast growth factor receptor 1-3 kinase inhibitor, in patients with advanced solid tumors harboring genetic alterations in fibroblast growth factor receptors: Results of a global phase I, dose-escalation and dose-expansion stud. *J Clin Oncol* **35**:157–165.
- Omura T, and Sato R (1964) the Carbon Monoxide-Binding Pigment of Liver Microsomes. I. Evidence. *J Biol Chem* **239**:2370–2378.
- Pearson JT, Wahlstrom JL, Dickmann LJ, Kumar S, Halpert JR, Wienkers LC, Foti RS, and Rock DA (2007) Differential time-dependent inactivation of P450 3A4 and P450 3A5 by raloxifene: A key role for C239 in quenching reactive intermediates. *Chem Res Toxicol* **20**:1778–1786.
- Polasek TM, and Miners JO (2006) Quantitative prediction of macrolide drug-drug interaction potential from in vitro studies using testosterone as the human cytochrome P4503A substrate. *Eur J Clin Pharmacol* **62**:203–208.
- Polasek TM, and Miners JO (2008) Time-dependent inhibition of human drug metabolizing cytochromes P450 by tricyclic antidepressants. *Br J Clin Pharmacol* **65**:87–97.
- Pruksaritanont T, Ma B, Tang C, Meng Y, Assang C, Lu P, Reider PJ, Lin JH, and Baillie TA (1999) Metabolic interactions between mibefradil and HMG-CoA reductase inhibitors: an in vitro investigation with human liver preparations. *Br J Clin Pharmacol* **47**:291–298.
- Reyes M, Belcher V, Hormel K, Chung D, Guptha S, Zamora C, Atiee G, Roupe K, Zhang W, Moran S, Martin D, and Stark J (2020) PII-053 Drug Interaction Potential Of Infigratinib (BGJ398), A Potent and Selective FGFR1–3 Inhibitor, in Healthy Volunteers (HV): Pharmacokinetics (PK) and Safety. *Clin Pharmacol Ther* **107**:S49–S50.
- Sevrioukova IF, and Poulos TL (2013) Understanding the mechanism of cytochrome P450 3A4: Recent advances and remaining problems. *Dalton Trans* **42**:3116–3126.
- Short NJ, and Connors JM (2014) New Oral Anticoagulants and the Cancer Patient. *Oncologist* **19**:82–93.
- Silverman RB (1995) Mechanism-based enzyme inactivators. *Methods Enzymol* **249**:240–283.
- Stephens C, Andrade RJ, and Lucena MI (2014) Mechanisms of drug-induced liver injury. *Curr Opin Allergy Clin Immunol* **14**:286–292.
- Tang LWT, Teng JW, Koh SK, Zhou L, Go ML, and Chan ECY (2021a) Mechanism-

- Based Inactivation of Cytochrome P450 3A4 and 3A5 by the Fibroblast Growth Factor Receptor Inhibitor Erdafitinib. *Chem Res Toxicol* doi: 10.1021/acs.chemrestox.1c00178.
- Tang LWT, Verma RK, Fan H, and Chan ECY (2021b) Mechanism-Based Inactivation of Cytochrome P450 3A4 by Benzbromarone. *Mol Pharmacol* **99**:266–276.
- Tang LWT, Verma RK, Yong RP, Li X, Wang L, Lin Q, Fan H, and Chan ECY (2021c) Differential Reversible and Irreversible Interactions between Benzbromarone and Human Cytochrome P450s 3A4 and 3A5. *Mol Pharmacol* doi: 10.1124/molpharm.121.000256.
- Teng WC, Oh JW, New LS, Wahlin MD, Nelson SD, Ho HK, and Chan ECY (2010) Mechanism-based inactivation of cytochrome P450 3A4 by lapatinib. *Mol Pharmacol* **78**:693–703.
- Turner N, and Grose R (2010) Fibroblast growth factor signalling: From development to cancer, *Nat Rev Cancer* **10**:116–129.
- Watanabe A, Nakamura K, Okudaira N, Okazaki O, and Sudo KI (2007) Risk assessment for drug-drug interaction caused by metabolism-based inhibition of CYP3A using automated in vitro assay systems and its application in the early drug discovery process. *Drug Metab Dispos* **35**:1232–1238.
- Williams PA, Cosme J, Matak Vinković D, Ward A, Angove HC, Day PJ, Vonrhein C, Tickle IJ, and Jhoti H (2004) Crystal structures of human cytochrome P450 3A4 bound to metyrapone and progesterone. *Science* **305**:683–686.
- Zanger UM, and Schwab M (2013) Cytochrome P450 enzymes in drug metabolism: Regulation of gene expression, enzyme activities, and impact of genetic variation. *Pharmacol Ther* **138**:103–141.
- Zanger UM, Turpeinen M, Klein K, and Schwab M (2008) Functional pharmacogenetics/genomics of human cytochromes P450 involved in drug biotransformation. *Anal Bioanal Chem* **392**:1093–1108
- Zhu K, Borrelli KW, Greenwood JR, Day T, Abel R, Farid RS, and Harder E (2014) Docking covalent inhibitors: A parameter free approach to pose prediction and scoring. *J Chem Inf Model* **54**:1932–1940.

FOOTNOTES

This work was supported by the Agency for Science, Technology and Research (A*STAR) Industry Alignment Fund – Pre-Positioning (IAF-PP) [Grant H18/01/a0/C14] and the Joseph Lim Boon Tiong Urology Cancer Research Initiative [Grant: R-148-000-302-720] to E.C.Y.C. L.W.T.T is supported by the National University of Singapore (NUS) President's Graduate Fellowship (PGF).

The authors declare that they have no conflicts of interest with the contents of this article.

FIGURE LEGENDS

Fig. 1. Chemical structure of infogratinib (INF)

Fig. 2. Substrate depletion of INF by CYP3A. Percentage of INF remaining against time in the presence of (A) CYP3A4 and (B) CYP3A5 plotted on a linear scale and the corresponding substrate depletion graphs of INF in the presence of (C) CYP3A4 and (D) CYP3A5 as plotted on a semi-natural logarithmic scale. Each point in (A to D) represents the mean and S.D. of triplicate experiments.

Fig. 3. Time- and concentration-dependent inactivation of CYP3A4 by INF using (A) testosterone, (B) midazolam and (C) rivaroxaban as probe substrates. Nonlinear regression of observed first-order inactivation rate constants (k_{obs}) versus INF concentration yielded K_i and k_{inact} values of $3.26 \pm 0.61 \mu\text{M}$ and $0.027 \pm 0.002 \text{ min}^{-1}$ when (D) testosterone was utilized as the probe substrate, $9.03 \pm 2.85 \mu\text{M}$ and $0.088 \pm 0.011 \text{ min}^{-1}$ when (E) midazolam was harnessed as the probe substrate and $4.17 \pm 0.93 \mu\text{M}$ and $0.068 \pm 0.005 \text{ min}^{-1}$ when (F) rivaroxaban was employed as probe substrates respectively. Each point in (A to C) represents the mean and S.D. of triplicate experiments.

Fig. 4. Cofactor NADPH-dependent inactivation of CYP3A4 by INF using (A) testosterone and (B) midazolam as probe substrates. Each point in (A and B) represents the mean and S.D. of triplicate experiments.

Fig. 5. (A) Partition ratio for the inactivation of CYP3A4 by INF estimated to be 41 was determined by extrapolating the intercept of the linear regression line at lower ratios and the straight line for the high ratios to the x-axis. Inactivation of CYP3A4 was attenuated in the presence of (B) an alternative CYP3A substrate testosterone (TES) and (C) a direct CYP3A inhibitor ketoconazole (KTC). (D) Conversely, the presence

of either GSH or catalase did not protect against enzymatic inactivation. Each point in (A to D) represents the mean and S.D. of triplicate experiments.

Fig. 6. (A) Percentage activity of CYP3A4 remaining did not increase after extensive dialysis at 4°C for 4 h. (B) Potassium ferricyanide (KFC) only restored the metabolic activity of CYP3A4 by a modest $4.8 \pm 1.11\%$ after a 30 min incubation with 25 μM INF. Results from both graphs show the mean and S.D. of two independent experiments conducted in triplicates.

Fig. 7. (A) Spectral difference measured over 60 min failed to elicit a Soret peak in the absorbance ranges of 448 – 458 nm for CYP3A4 incubated with 25 μM INF. (B) Similarly, a comparison of the absorbance at the reference of 454 nm against the isosbestic point at 490 nm failed to demonstrate an increase in the extent of MI complex formation over time. (C) Reduced CO-difference spectrum of CYP3A4 following incubation with 25 μM INF for 30 min in the absence and presence of cofactor NADPH.

Fig. 8. Proposed accurate mass fragmentation pattern of the INF-derived GSH adduct. The MS/MS spectrum depicts the experimental m/z values whereas the chemical structure illustrates the theoretical accurate m/z values of the parent and product ions of the adduct as outlined in Table 2 using a mass tolerance of 5 ppm.

Fig. 9. Covalent adduction of INF to CYP3A4 and CYP3A5. Molecular plots illustrating the top scored binding poses for INF adducts at (A) Cys239 in the ‘closed’ conformation of CYP3A4 (PDB ID: 414H) and (B and C) Ser239 in both the ‘closed’ and ‘open’ conformations of CYP3A5 (cluster-13 and cluster-18 respectively). In all three instances, the 2,6-dichloro-3,5-dimethoxy-phenyl moiety of INF is visibly oriented towards the F-F’ loop.

Fig. 10. Dose-response curves depicting reversible inhibition elicited by INF against CYP3A4, using (A) testosterone, (B) midazolam and (C) rivaroxaban as probe substrates. The IC_{50} values obtained were 2.04 ± 0.29 , 2.91 ± 0.54 and 0.80 ± 0.079 μ M respectively. Each point in (A to C) represents the mean and S.D. of triplicate experiments.

Fig. 11. Reversible inhibition of CYP3A4 by INF using rivaroxaban as the probe substrate. (A) The formation rate of hydroxylated rivaroxaban (expressed in peak area ratio) was plotted against inhibitor concentration and fitted in the Michaelis-Menten kinetic model which determined K_i to be 0.97 ± 0.06 μ M. (B) Lineweaver-Burk plot revealed the mode of inhibition to be noncompetitive. Each point in (A and B) represents the mean and S.D. of triplicate experiments.

Fig. 12. Proposed bioactivation pathways of INF by CYP3A4.

Table 1. CYP3A4 inactivation kinetic parameters for INF derived using either testosterone 6 β -hydroxylation, midazolam 1'-hydroxylation or morpholinone hydroxylation of rivaroxaban as surrogate markers of residual CYP3A activity. Data are presented as means \pm S.D.

Probe Substrate	K_i (μM)	k_{inact} (min^{-1})	k_{inact}/K_i ($\text{min}^{-1}\text{mM}^{-1}$)	$t_{1/2}$ (min)	Partition Ratio
Testosterone	3.26 \pm 0.61	0.027 \pm 0.002	8.4	25.40	N.D
Midazolam	9.03 \pm 2.85	0.088 \pm 0.011	9.8	7.85	N.D
Rivaroxaban	4.17 \pm 0.93	0.068 \pm 0.005	16.4	10.12	41

N.D: not determined

Table 2. Accurate mass measurement of the parent and product ions of INF-derived GSH adduct (m/z 865) using a mass tolerance of 5 ppm.

Proposed Elemental Composition	Theoretical m/z	Experimental m/z	Mass Accuracy	
			ΔDa	Δppm
$C_{36}H_{46}N_{10}O_9SCl_2$	865.2620	865.2599	-0.0021	-2.4
$C_{36}H_{44}N_{10}O_8SCl_2$	847.2514	847.2487	-0.0027	-3.2
$C_{31}H_{39}N_9O_6SCl_2$	736.2194	736.2176	-0.0018	-2.4
$C_{27}H_{39}N_9O_6S$	618.2817	618.2804	-0.0013	-2.1
$C_{27}H_{37}N_9O_5S$	600.2711	600.2689	-0.0022	-3.7
$C_{22}H_{32}N_8O_3S$	489.2391	489.2378	-0.0013	-2.6
$C_{17}H_{24}N_6S$	345.1856	345.1848	-0.0008	-2.3

Table 3. Summary of covalent docking scores for INF

P450 Isoform	Residue	PDB/Cluster ID	Docking Score	Minimum distance between INF and F-F' loop (Å)
CYP3A4	Cys239	4I4H [^]	-4.7 [#]	3.1
		4I3Q [^]	-4.6	3.3
		4K9W [^]	-4.4	3.0
		5A1P [^]	-4.1	3.3
		3NXU [^]	-4.1	3.3
		1TQN [^]	-3.4	3.1
CYP3A5	Ser239	Cluster-13 [^]	-5.4 [#]	3.1
		Cluster-18 [*]	-3.6	3.2

[#] PDB/Cluster ID with best covalent docking score for a given residue position.

[^] F-F' loop in 'closed' conformation (see Discussion).

^{*} F-F' loop in 'open' conformation (see Discussion).

Table 4. CYP3A4 reversible inhibition parameters for INF derived using either testosterone 6 β -hydroxylation, midazolam 1'-hydroxylation or morpholinone hydroxylation of rivaroxaban as surrogate markers of residual CYP3A activity. Data are presented as means \pm S.D.

Probe Substrate	IC₅₀ (μM)	K_i (μM)	Mode of Inhibition
Testosterone	2.04 \pm 0.29	N.D	N.D
Midazolam	2.91 \pm 0.54	N.D	N.D
Rivaroxaban	0.80 \pm 0.08	0.97 \pm 0.06	Noncompetitive

N.D: not determined

Table 5. Comparison of enzyme inactivation kinetic parameters between INF and several clinically-important MBI of CYP3A4 using testosterone 6 β -hydroxylation as a marker reaction of CYP3A activity.

Compound	K_i (μM)	k_{inact} (min^{-1})	k_{inact}/K_i ($\text{min}^{-1} \text{mM}^{-1}$)	Reference
INF	3.26	0.027	8.4	
Clarithromycin	2.25	0.04	17.8	Polasek and Miners, 2006
Diltiazem	0.5	0.01	20.0	Ma <i>et al.</i> , 2000
Mibefradil	2.3	0.4	173.9	Prueksaritanont <i>et al.</i> , 1999

Figure 1

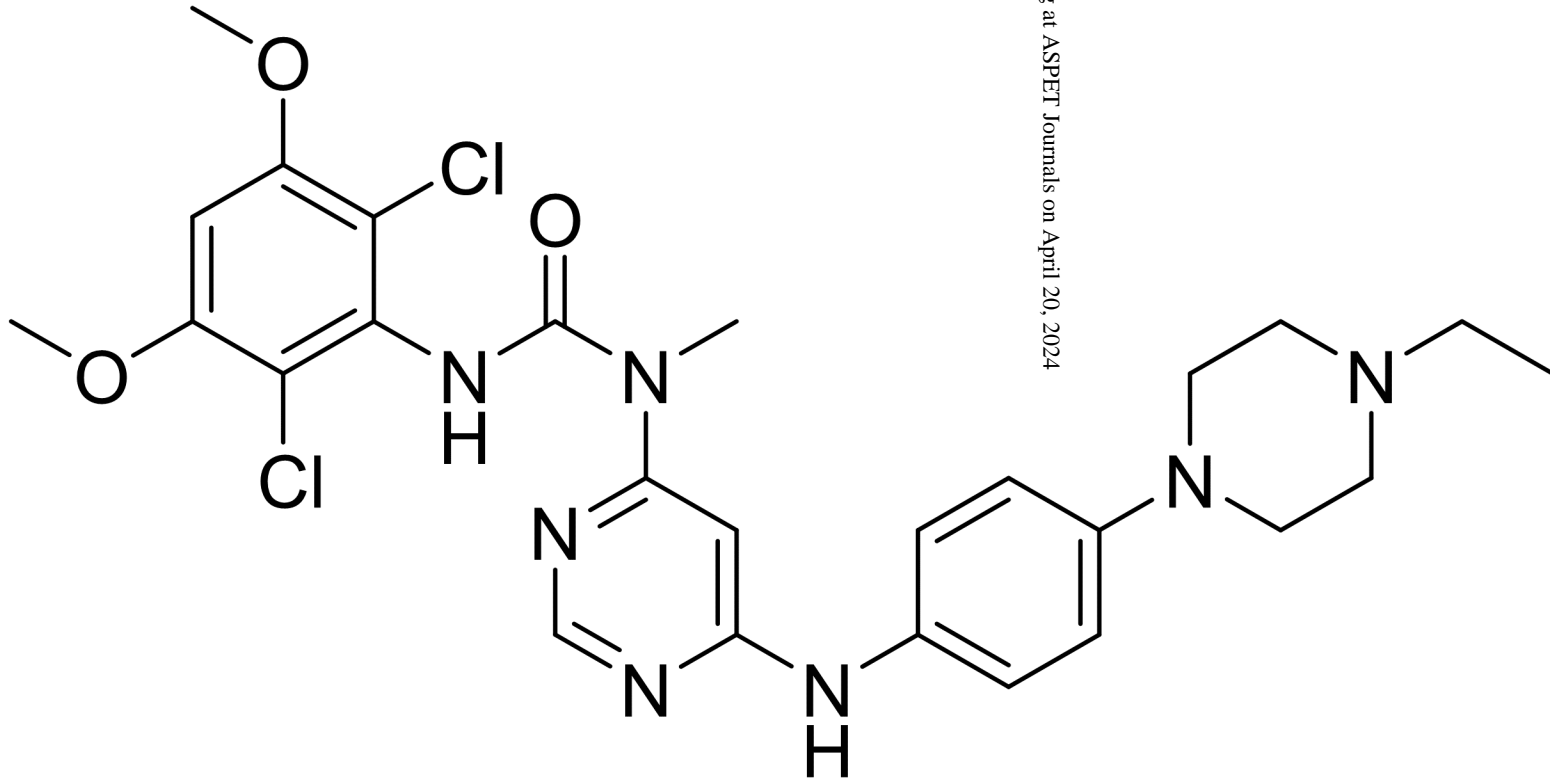
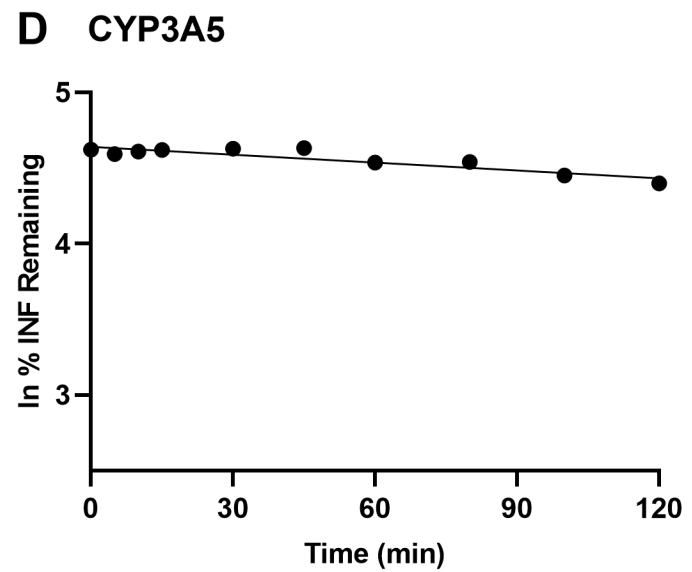
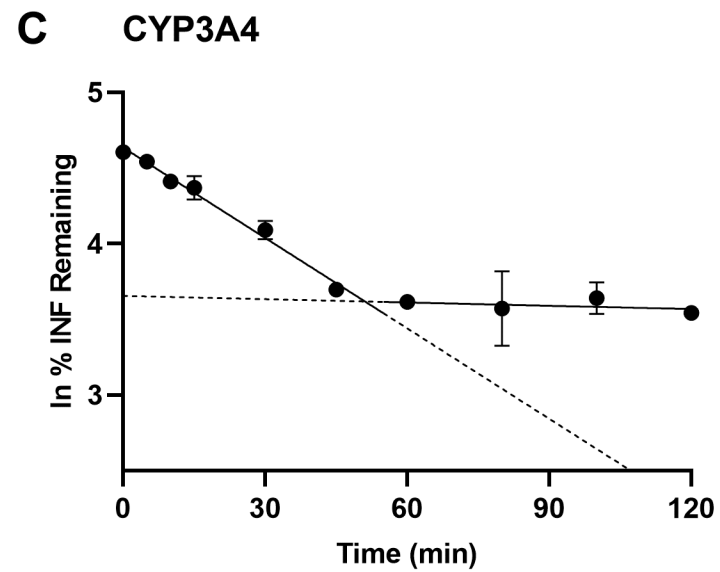
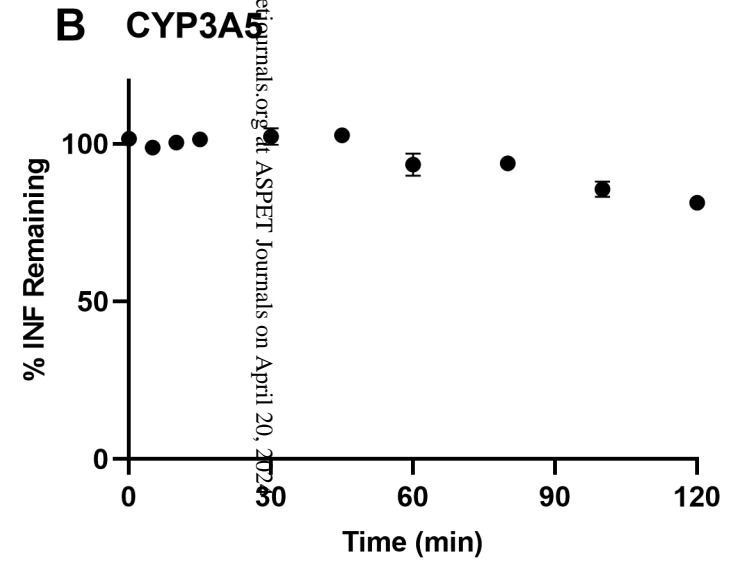
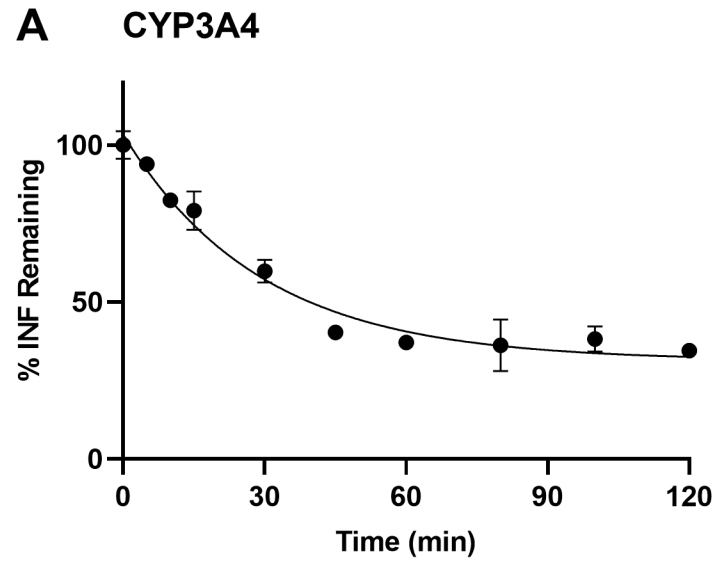


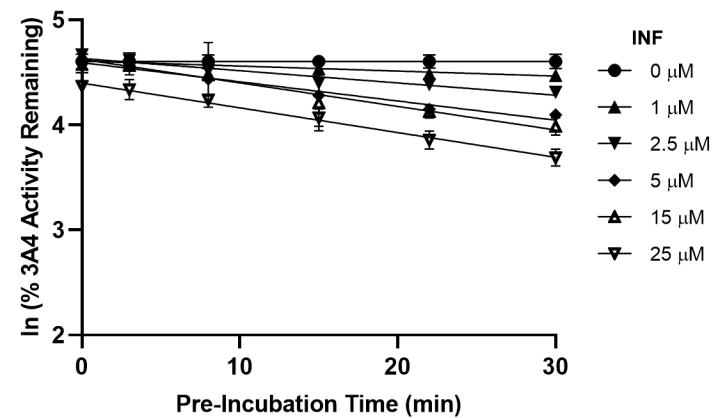
Figure 2



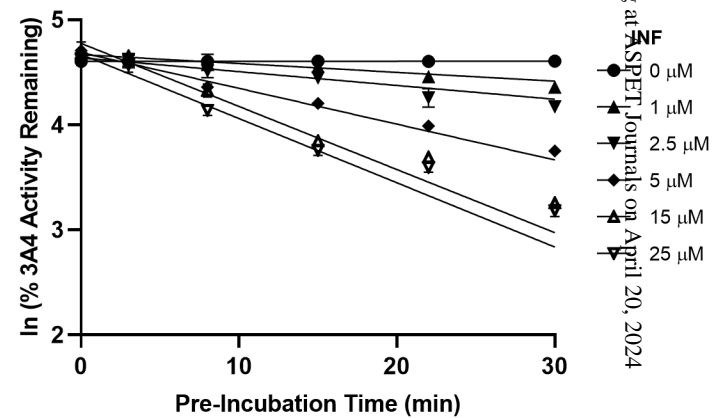
Downloaded from dmnd.aspetjournals.org at ASPET Journals on April 20, 2024

Figure 3

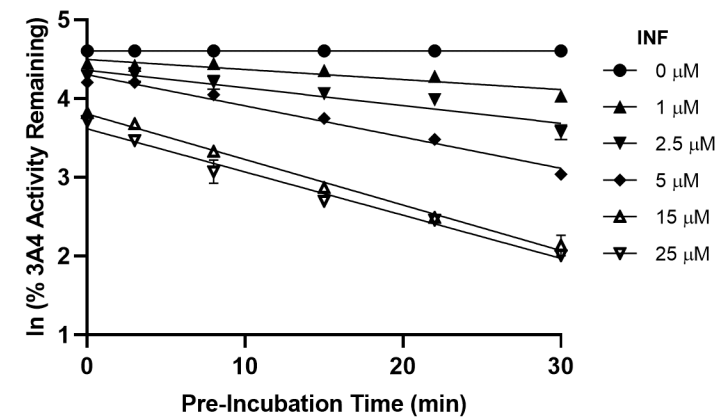
A Testosterone 6 β -Hydroxylation



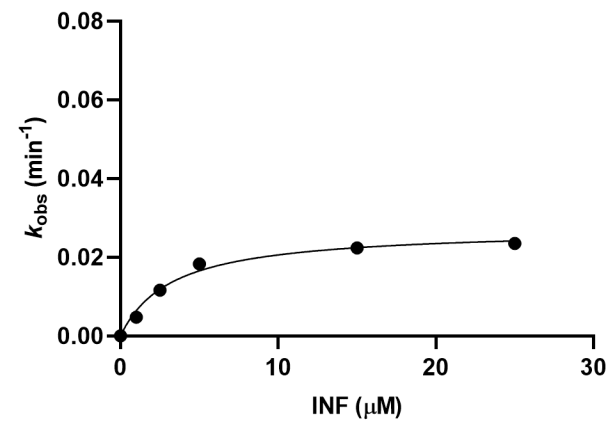
B Midazolam 1'-Hydroxylation



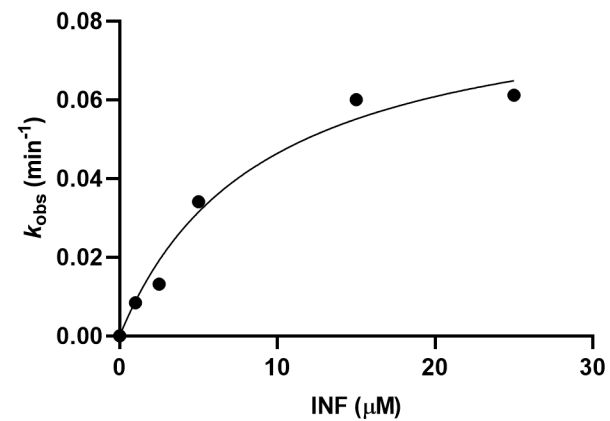
C Rivaroxaban Hydroxylation



D



E



F

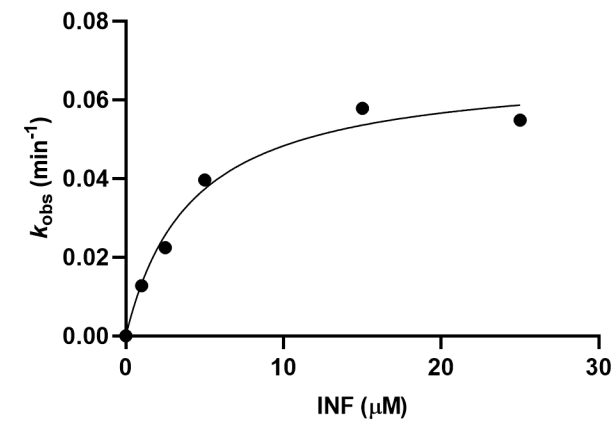
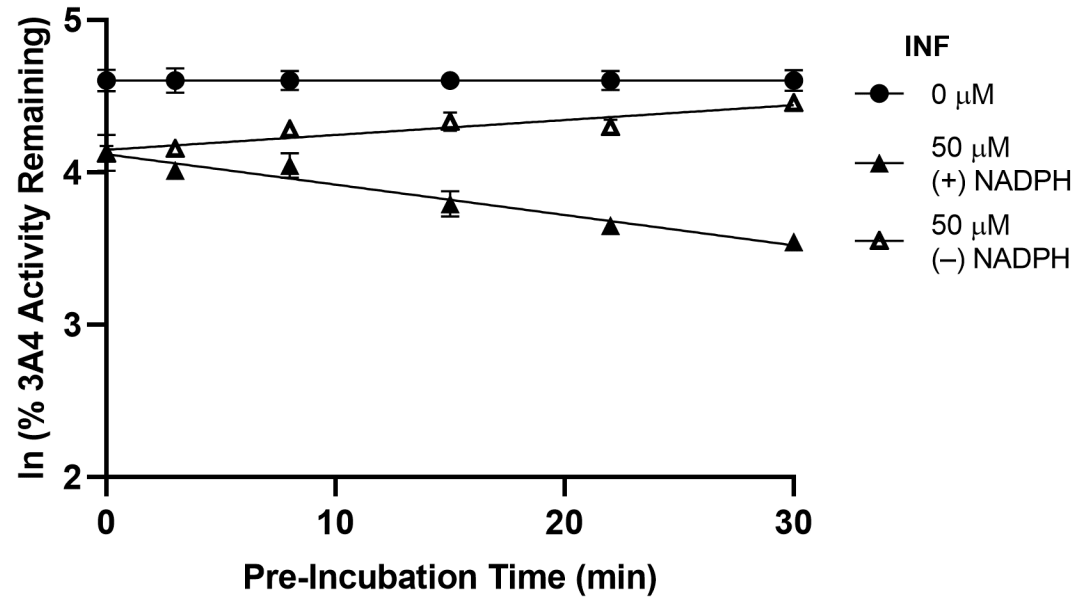
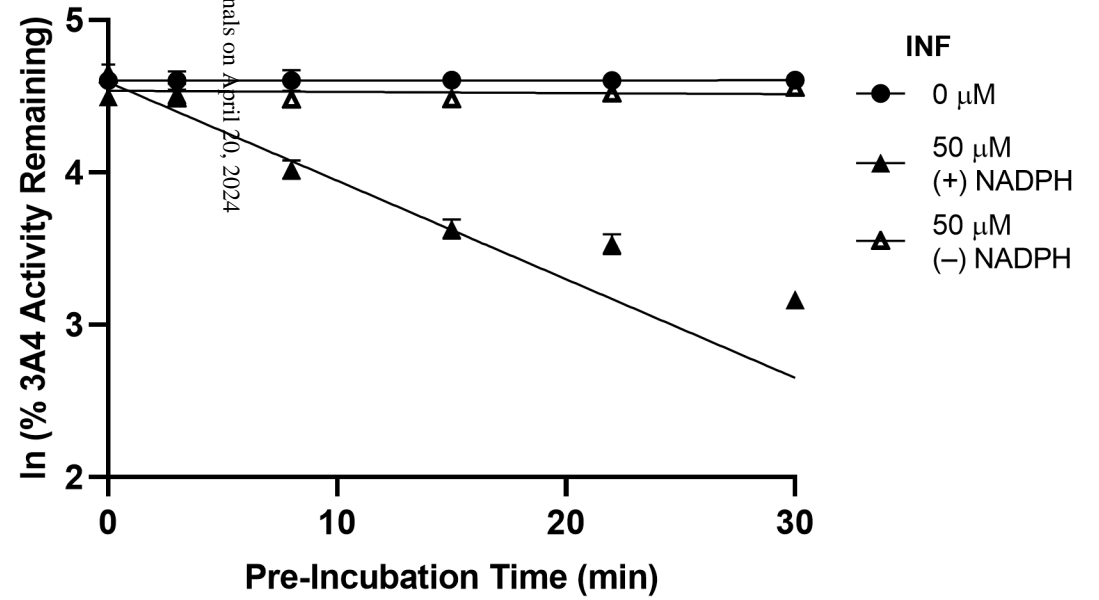


Figure 4

A Testosterone 6 β -Hydroxylation



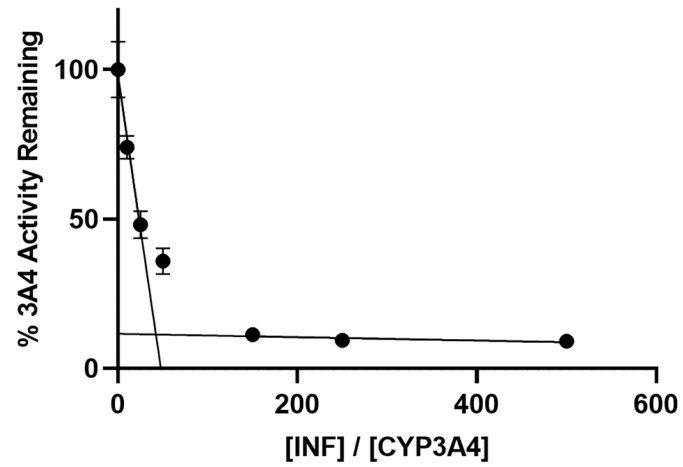
B Midazolam 1'-Hydroxylation



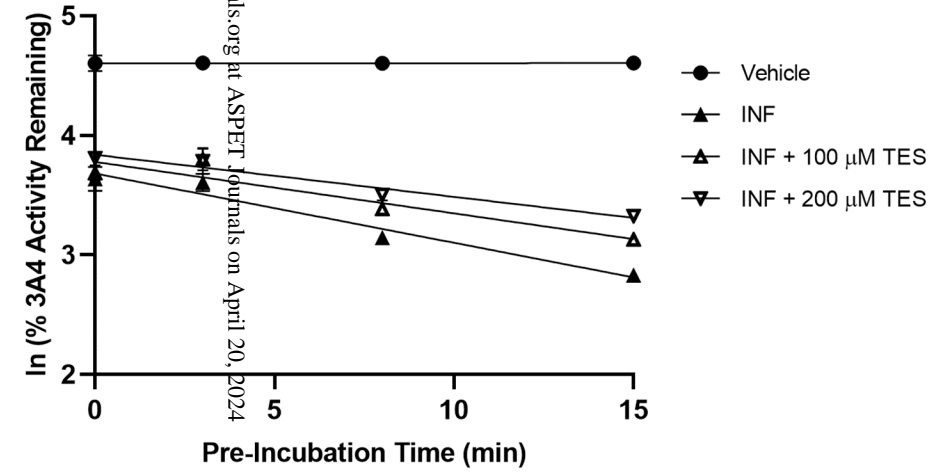
loaded from dmd.aspejournals.org at ASPET Journals on April 20, 2024

Figure 5

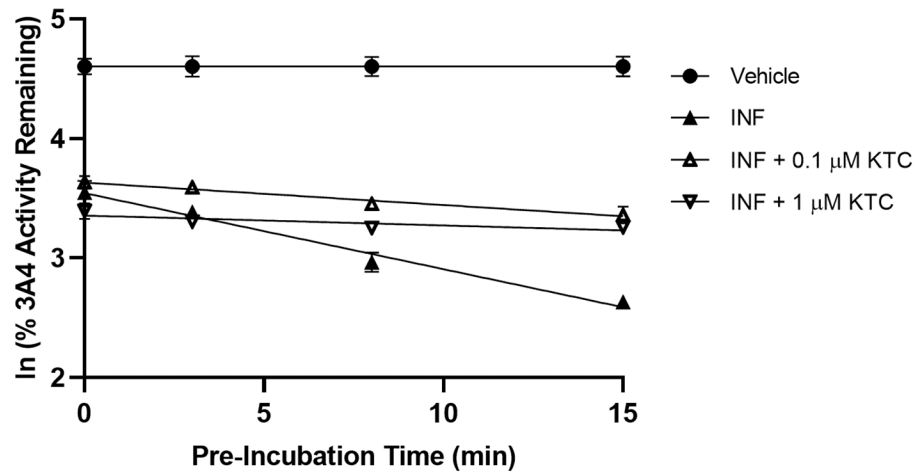
A



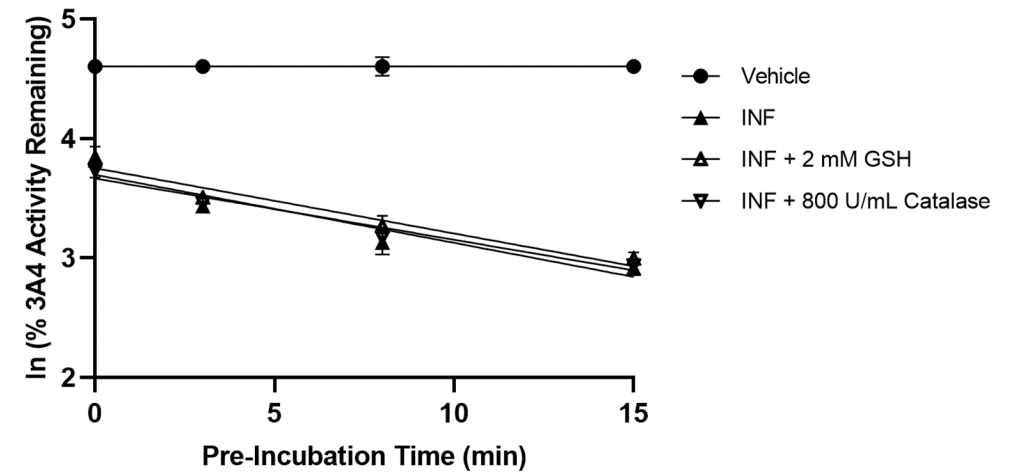
B



C



D



loaded from dnd.aspetjournals.org at ASPET Journals on April 20, 2024

Figure 6

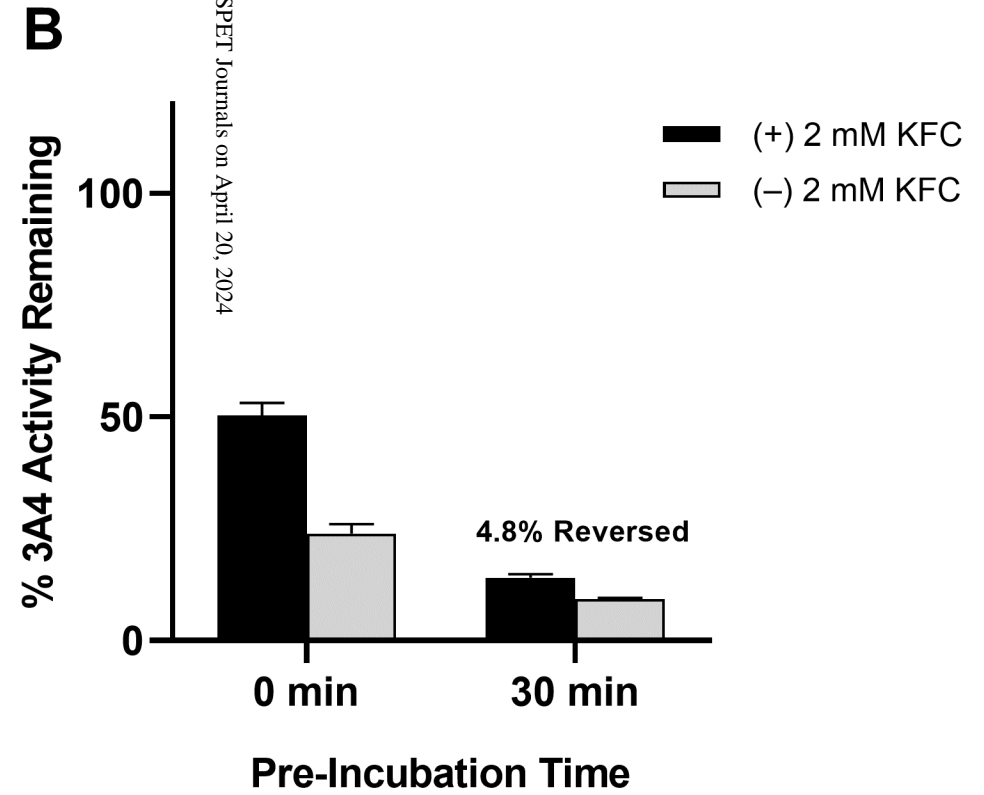
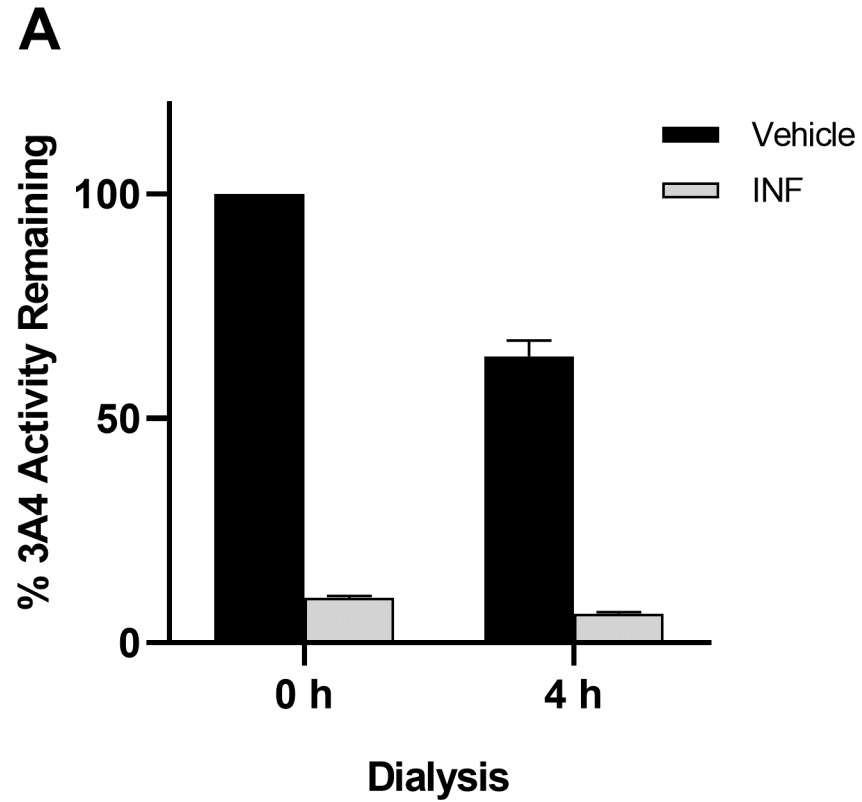
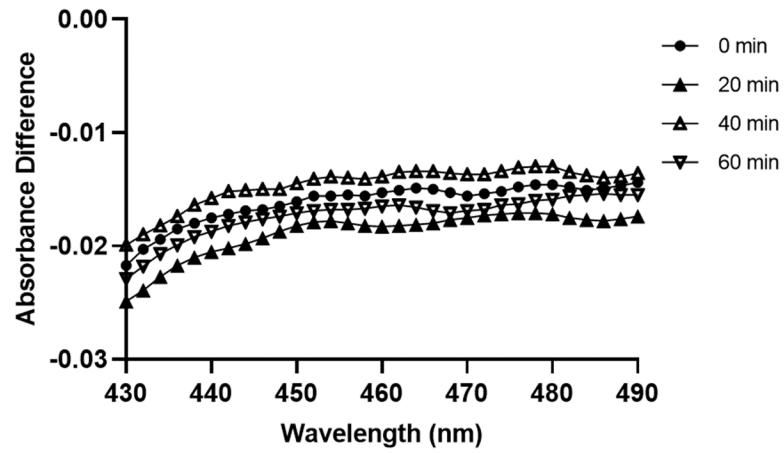
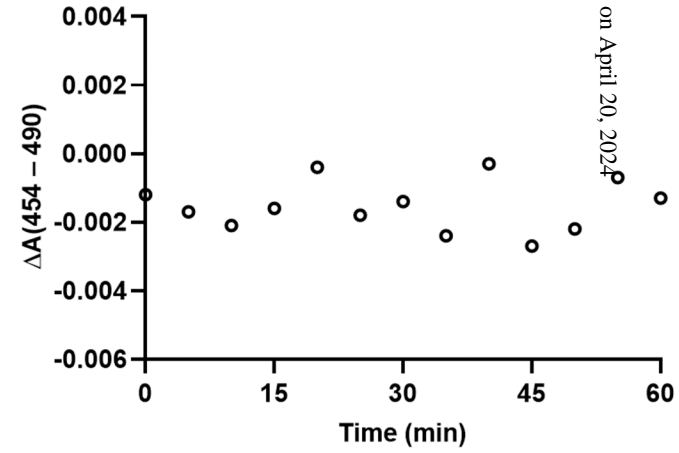


Figure 7

A



B



C

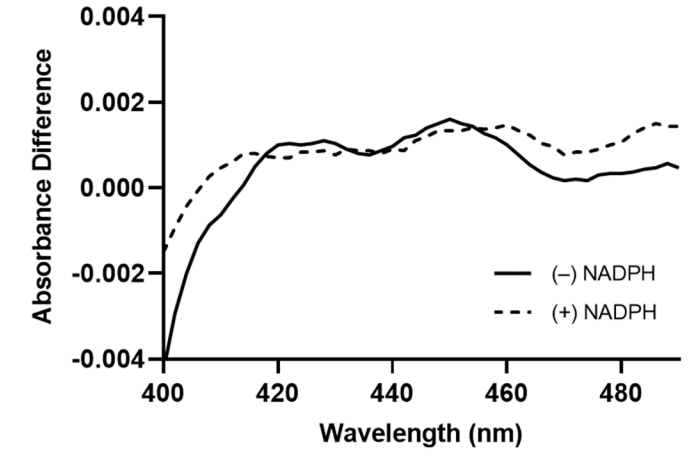
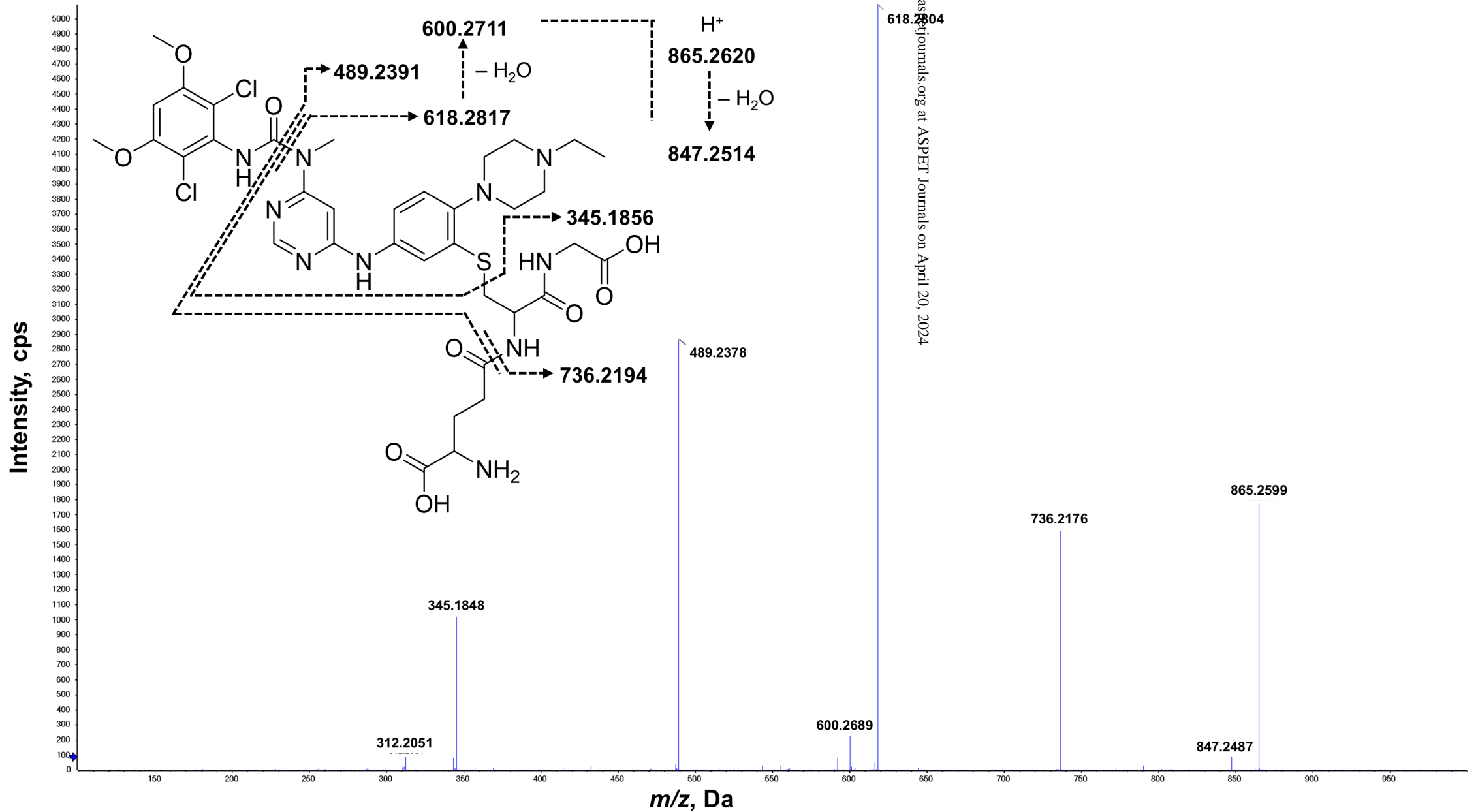


Figure 8



loaded from dmd.aspenjournals.org at ASPET Journals on April 20, 2024

Figure 9

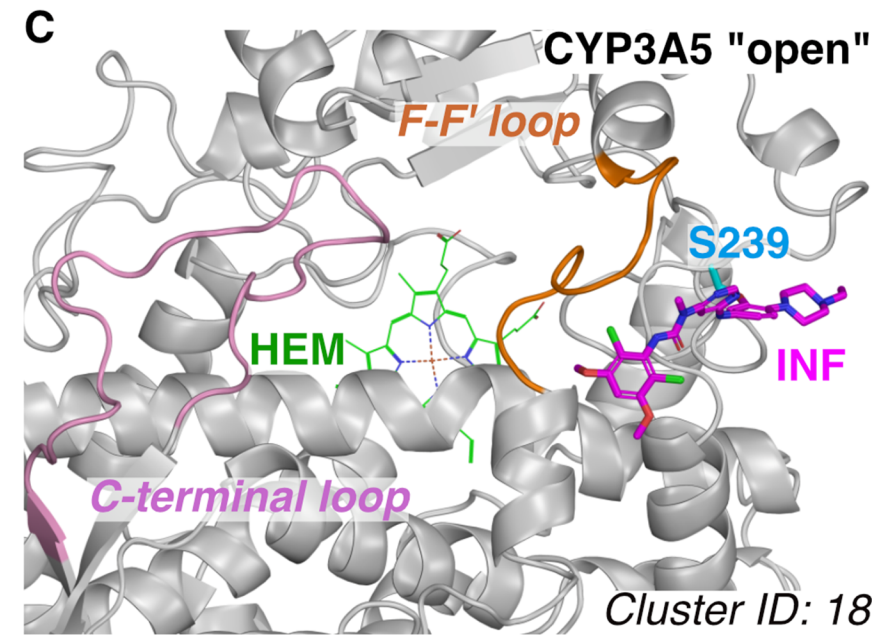
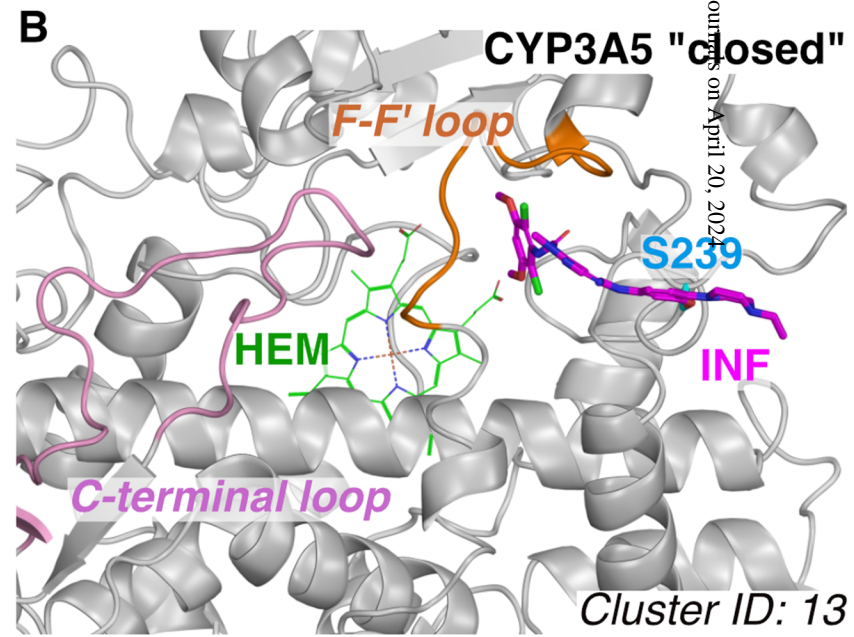
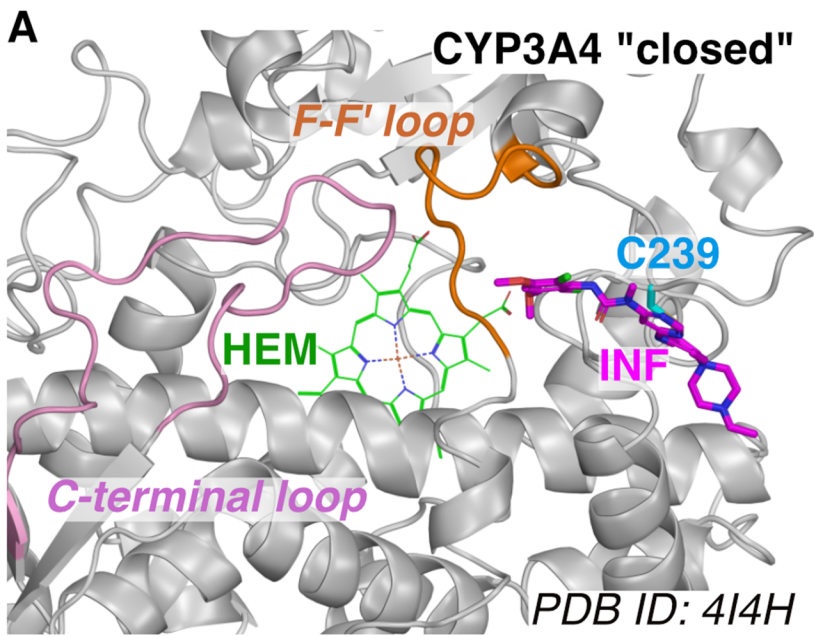
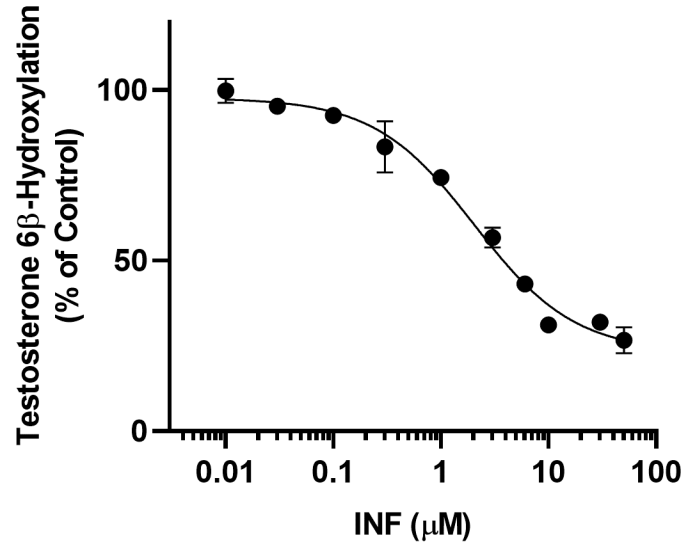
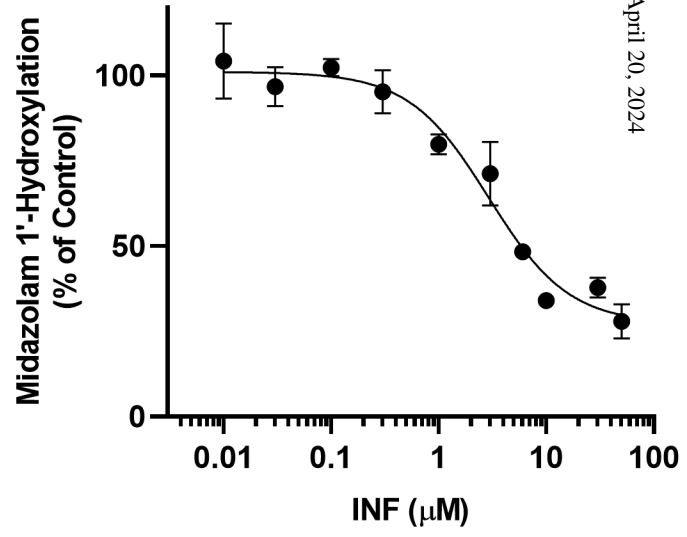


Figure 10

A



B



C

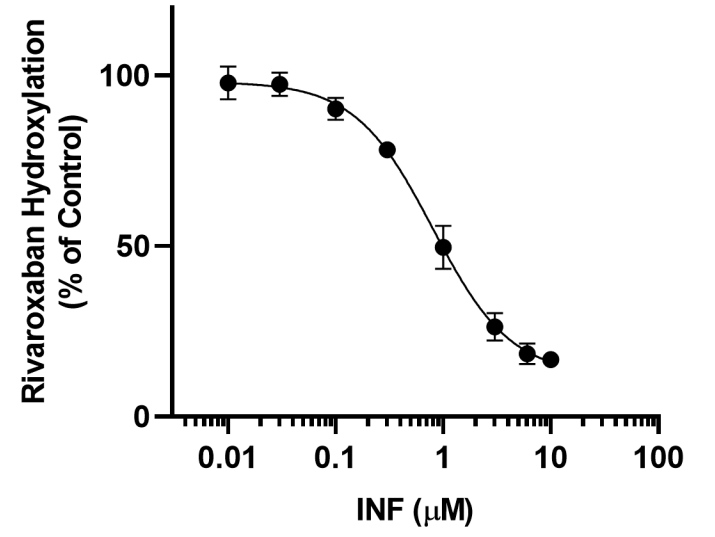
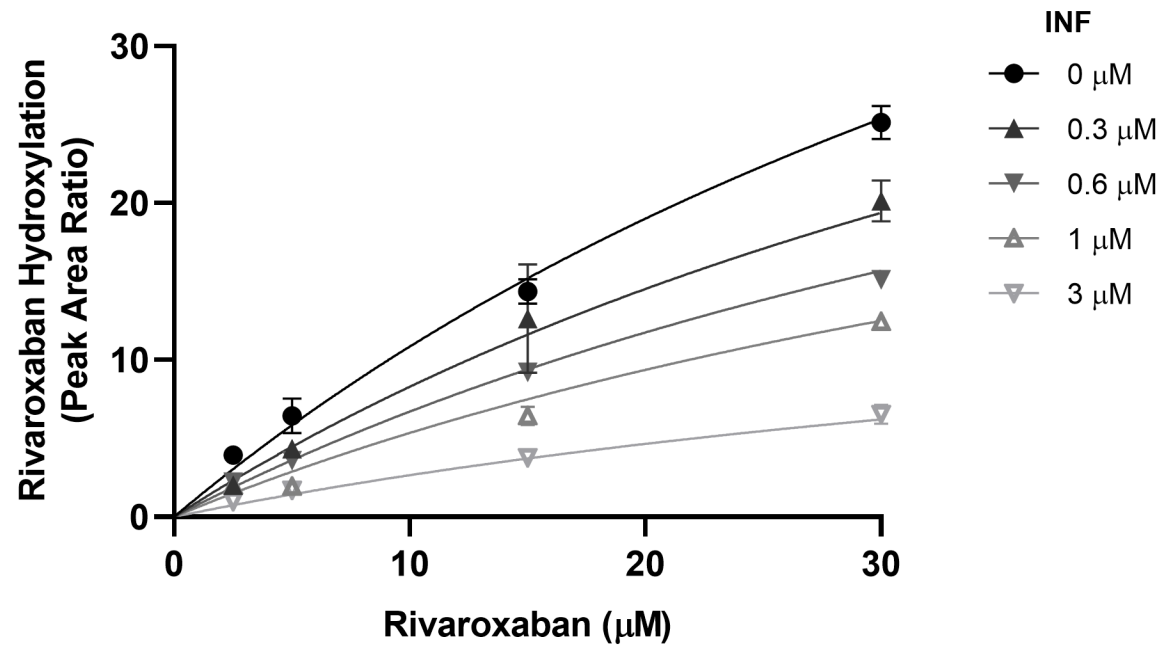


Figure 11

A



B

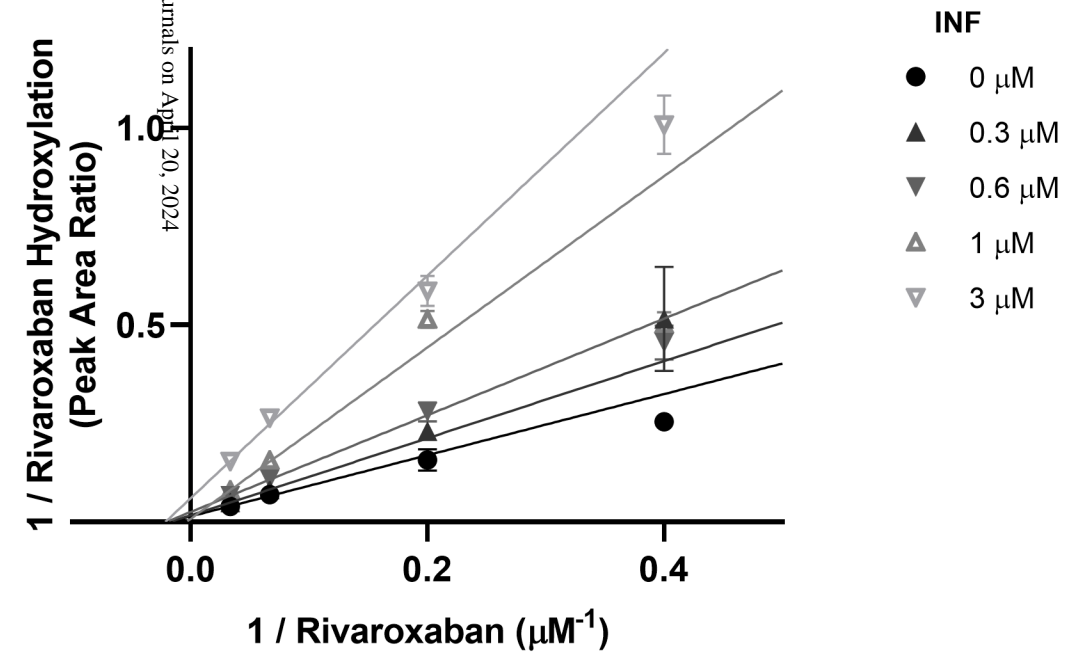


Figure 12

